63-3-2

Interim Scientific Report No. 4

Contract AF 33(657)-8311

LONG LIFE CLOSED LOOP MHD RESEARCH AND DEVELOPMENT UNIT

Period Covered:

December 15, 1962 to March 15, 1963

March 15, 1963

Interim Scientific Report No. 4

Contract AF 33(657)-8311

Long Life Closed Loop MHD Research and Development Unit

Period Covered:

December 15, 1962 to March 15, 1963

March 15, 1963

Westinghouse Electric Corporation
Research and Development Center
Pittsburgh 35, Pennsylvania

The effort depicted in this report is sponsored by the Aeronautical Systems Division (Flight Accessories Laboratory, ASRMF) of the United States Air Force.

The work covered by this report was accomplished under Air Force Contract AF 33(657)-8311, but this report is being published and distributed prior to Air Force review. The publication of this report, therefore does not constitute approval by the Air Force of the findings or conclusions contained herein. It is published for exchange and stimulation of ideas.

Table of Contents

Table of Contents (Cont'd)

I. Introduction

The major components of the MHD loop have been delivered to the assembly area and the main effort of the group is now concentrated on problems of assembly and preliminary testing of the various portions of the equipment. We are therefore in a position to report on component evaluation and performance of most of the auxiliary apparatus. Due to the expected complexity of the actual testing of the loop and the possibility of extensive damage which may result from improper operation, very careful and detailed attention is being paid to the proper installation and functioning of all parts of the experiment. In addition, a safety survey was made and every reasonable precaution is being taken to insure that personnel will not be hurt in case of an accident. This includes the modification of the present building and rearrangement of the existing equipment.

II. Overall Status of Project

It is presently expected that the closed loop will be in operation within the next two months. This is, however approximately three months (25%) behind the originally planned schedule.

During this quarter most of the effort has been concentrated on assembly of the loop and its auxiliaries as well as testing, evaluating and revising the auxiliaries.

Many of the instruments such as rheostats, ammeters, voltmeters, potentiometers, etc. have been installed in the control panel. The extensive job of electrically wiring between the control panel and the loop will be started within the next two weeks.

The complete cesium monitoring system has been successfully operated as a bench setup. It will now be dismantled and reassembled on appropriate panels for operation on the bleed flow from the loop.

An electrical conductivity probe, having simplicity of design, has been built and given preliminary testing in water solutions of known conductivity. The probe will be further tested in a glow discharge tube and on the small MHD generator before being applied on the closed loop.

Minor changes have been made in the two magnets for the closed loop and they have now been recalibrated and are ready for use. The magnets as well as other auxiliaries of the loop will be described and discussed in later sections of this report.

III. Refinements in Design and Instrumentation

The main reason that the project has consumed both more time and money than was originally anticipated is due to the refinements in design and instrumentation which were not conceived in the original plan. It is firmly believed, however, that the refinements which have been incorporated since the original plan will justify the additional effort. Some of the refinements are as follows:

Magnet current regulators have been designed and built to provide automatic precise magnetic flux control.

Probes are being made to continuously monitor the electrical conductivity of the plasma.

An automatic regulator has been built to control the output of a D.C. generator which in turn supplies current to a tantalum resistive heater for plasma temperature control.

The generator on the closed loop is designed as a segmented Faraday device. However, to make it function as a segmented Faraday device with no axial flow of current it has been necessary to provide guard electrodes at either end of the generator. These guard electrodes, which are located approximately 1/2 way between the ends of the generator and electrically grounded tantalum liner, will be supplied with the appropriate voltage so as to establish a zero axial electrical field between the ends of the generator and the guard electrodes. Appropriate power supplies and electric field sensing probes have been designed to accomplish this objective.

Originally it had been planned to series connect the 16 pairs of electrodes on the motor section so that a single high voltage power supply could be used. The power supply would have been relatively simple, but it would have correctly accommodated only one value of $\omega\tau$. To avoid this shortcoming, sixteen separate electrically isolated floating power supplies were built.

A system has been designed, built and tested for monitoring the concentration of cesium in the cesium-helium working fluid of the closed loop. This monitoring system analyzes a small bleed flow from the loop. The loop is provided with a continuous known makeup flow of both helium and cesium so as to establish the bleed flow. The monitoring system was built because it is expected that the cesium-helium concentration in the makeup flow will not be representative of the working fluid. Some of the cesium may be adsorbed and absorbed within the loop.

IV. Safety Considerations

A concentrated effect is being made to eliminate the hazards associated with the operation of the closed loop. An additional brick room attached to the present building has been constructed to house the small straight through MHD generator and work-top cabinets which are now in the present building. However it is unnecessary to relocate its control panel because of the proximity of the addition. In its present location the tunnel blocks an escape exit which is necessary for safe operation of the loop. Also an additional safety exit is being installed. This expansion will give sufficient clearance on the sides of the MHD closed loop installation and escape routes at all four corners of the experimental area. Even after applying these safety considerations, strict procedures must be adhered to because of the potentially dangerous materials and the relatively limited space.

V. Conductivity Probes

The electrical conductivity of the ionized gas in an MHD generator or motor duct is a tensor quantity. The electrical conductivity parallel to the applied magnetic field is equal to the scalar conductivity and the effective conductivity transverse to the magnetic field is related to the scalar value by the following equation

$$\sigma_1 = \frac{\sigma_o}{1 + (\omega_b \tau)^2} \qquad (1)$$

where

σ_1 = transverse conductivity in mho/m

σ_o = scalar conductivity in mho/m

ω_b = electron cyclotron frequency in cps

τ = mean electron collision time in seconds

Therefore a measurement of the scalar conductivity is needed in order to check the theoretical values given in the literature.[1] Two types

---

1) L. S. Frost, Journal of Applied Physics, Vol. 32, No. 1, 2029-2036, October 1961.

of probes are being investigated. The first probe known as a double probe consists of two parallel thin wires inserted into the plasma and the electrical resistance between them is measured by a low frequency a-c bridge. With a resistance versus conductivity calibration curve, the conductivity of the plasma is easily determined. The second probe is an eddy current probe which consists of a coil of wire extended into the plasma and the Q of the coil is measured. With a Q versus conductivity calibration curve, the conductivity of the plasma is determined. The conductivity readings of the first probe are more directional than the second; therefore, the first probe measures separately the conductivities parallel and transversed to the magnetic field by rotation of the probe. From these two measurements, the electron mobility of the gas can be calculated. The magnetic field must be turned off in order that the second probe will measure the scalar conductivity.

Two double probes have been constructed and tested in conducting liquids. Figure 1 shows the construction of the probe and Figure 2 shows their placement in the MHD closed loop generator-motor. The probe consists of two parallel tungsten wires fed through a ceramic insulating tube. The tube is coated with a high Q dope to prevent the ceramic being penetrated with the conducting liquid. Otherwise the probe will give a false reading. The tungsten wires are plated with platinum black to reduce the polarization effect that occurs in

highly conductive liquids. An Electro-measurements, Inc. Model 250-DA 1000 cps impedance bridge was used to measure the resistance of the probes in KCl solutions. Each solution has a different concentration of KCl so that a range of conductivities from 3.7×10^{-2} to $1.54 \times 10^{+1}$ mho/m was covered. Figure 3 shows the experimental results of resistance versus conductivity for two double probes. One double probe has a wire diameter of .0655 in. and the other double probe has a wire diameter of .015 in. The theoretical values of resistance are plotted on the graph for comparison. Theoretical values of resistance were calculated from an equation based on the conductance per length between two infinitely long parallel wires. These values show that the measurements are in the correct order of magnitude; however, the difference is due to the fact that the wires of the probe have a finite length.

Temperature, vibration, and stress analysis was performed on the 15 mil diameter wire double probe. The results of the temperature analysis shows that the wire temperature should be approximately 1927°C when the gas temperature is 2000°C and the walls of the MHD duct are 1560°C. The calculations, which are for the worse case, indicate that change in conductivity in the vicinity of the wires should be negligible compared to the gas in the stream. The natural vibration frequency of the wires is about 400 times less than the excitation frequency produced by Karmon Vortices. The stress produced by the

dynamic pressure of the gas on the wires at their rigid end is about 10^5 times less than the maximum stress of the wires and the maximum deflection of a wire is less than 4 mils. This deflection should have negligible effect on the resistance measurements.

Materials have been ordered for the construction of a double probe to be used in the 3/4 in. MHD generator duct. However, first the probe will be tested in a helium-cesium discharge tube.

Several eddy-current probes[2] were constructed by L. S. Frost and are now being investigated. These probes are coupled to a grid dip meter as shown in Figure 4. The dip in grid current at the resonance frequency of the probe decreases with increasing conductivity of the media in which the probe is inserted. Preliminary experiments indicate that this probe may be a feasible instrument to measure conductivity. An advantage of this probe is that space charge sheaths and temperature boundary layers at the surface of the probe should have less influence on the conductivity measurements than that of the double probe. A disadvantage is that the probe scalar conductivity measurements must be made in the absence of the magnetic fields.

VI. Microwave Diagnostics for MHD Plasma

An investigation of microwave techniques to measure the electron collision frequency and electron and ion densities will be

---

2) E. C. Lary and R. A. Olson, Review of Scientific Instruments, Vol. 33, No. 2, 1350, December 1962.

made. Since the microwave generator signal detectors and associated hardware are external to the MHD duct, windows must be inserted in the duct walls to allow the microwaves to pass through the duct walls and into the plasma. Since these walls operate at temperatures from 1000 - 2000°C, it is difficult to obtain materials which are transparent to microwaves. Therefore, an investigation of the microwave properties of materials at high temperatures is planned.

Since the electron and ion densities in the MHD loop will be approximately 10^{19} m^{-3}, the microwave wavelength will be on the order of 4 to 8 mm, in order to operate above the plasma frequency. The materials to be investigated are SiO_2, MgO, Al_2O_3 and various compounds of these. The samples will be cut to one-half wavelength in thickness and inserted in a rig which will be connected to the wave guides; therefore reflected waves at the boundaries of the window should be reduced. This apparatus eventually may become an integrated part of the loop. Provisions are planned to heat the samples to temperatures which simulate the duct temperature. Measurements of the conductivity, dielectric constant, attenuation, and reflectivity of the material will be made as a function of temperature. Then the best material will be selected for the window.

An investigation of the interaction of microwaves and acoustical waves to measure the velocity of the plasma is planned. Other methods of velocity measurements will be considered.

VII. Argon Purge and Cooling System for Return Bend

A system has been devised to circulate argon through the annular zirconia bed between the tantalum liner and stainless steel jacket at the return bend. The argon flow achieves a two-fold purpose:

1) Gaseous contaminants can be purged out of the cavity, and
2) A means of heat extraction is provided.

Figure 5 shows a schematic of the system. The annular cavity in the return bend will be filled with .060 inch bubble zirconia grains. Reference 3 shows experimentally that the bed may be considered fixed if,

$$u_o << u_t$$

where u_o is the superficial fluid velocity, and

u_t is the terminal velocity of free-setting grain in the fluid.

Transition from a fixed to fluidized bed occurs generally for

$$u_o \simeq .1\, u_t$$

---

3) W. C. Lyon, S. Frank, M. R. Scheve, "Heat Transfer and Fluid Flow for Fluidized Bed Reactors," RP 603-31, Martin Nuclear Division.

In the zirconia bed u_o is less than .01 u_t and the pressure drop (Δp) may be calculated for fixed bed conditions and Reynold's number (Re) < 10 from the expression

$$\Delta p = \frac{2f\, G_o^2\, L\, (1-\epsilon)^2}{g\, D_p\, \rho_c\, \epsilon^3} \qquad (2)$$

where $f = \frac{100}{Re}$, friction factor

and G_o = superficial mass velocity of fluid

L = length of annular flow path

ϵ = porosity

g = gravitational constant

D_p = grain diameter

ρ_c = average fluid density in bed

On the basis of this relationship, 5 KW may be extracted by an argon flow circulated by a 1 H.P. turbine blower. The pressure drop in the bed is the largest contribution and absorbs about 40% of the available head. A bypass arrangement has been incorporated to allow continuous variation in flow through the bed from zero to full capacity of the blower.

Purging of the system will be accomplished in two stages in order that the getter tube may be reasonably compact. Argon will be

blown under supply pressure downward through the bed and exhausted to the atmosphere during warm-up, effecting the removal of a large fraction of the contaminants from the system. It would be too expensive however to provide direct cooling in this manner and the blower will be used after the initial purge. The getter tube will then handle the last traces of oxygen and nitrogen which collect in the argon stream. Fabrication of the system is in progress.

VIII. Compatibility of Tantalum and Cesium

Tests on the small straight through MHD tunnel have given evidence of impending difficulty with the tantalum liner of the closed loop. Some of the tantalum components of the small tunnel show an apparent incompatibility of tantalum and cesium. Considering the cost of the tantalum liner, there is great concern.

Cesium is brought into the small tunnel through a small tantalum tube connected to the positive displacement cesium feeder. The small tantalum tube extends into the mixing section approximately 3 inches downstream of the plasma generator. The cesium, transported by helium, is in the liquid state as it enters the tunnel through the tantalum tube. It is this small tube which has shown the greatest amount of corrosion. The hottest portion of the tube which extended through the zirconia lining of the mixing chamber was completely corroded away. The corrosion was progressively less severe on the

cooler portions of the tube extending through the ceramic. A section of the tube which was partially corroded away is being photomicrographed to determine whether the attack was on both the inside and outside of the tube. In addition, spark spectrographic techniques are being employed to determine the nature of the attack. The corrosive attack evidenced on the small tunnel is the cause of considerable concern in that the geometrical arrangement of the injector tube on the small tunnel is almost identical to that which is planned for the closed loop.

There has also been a corrosive attack on the electrodes of the generating section of the tunnel. This attack has manifested itself by producing wart-like protrusions on the electrode surfaces. Some of these warts have been removed for spectrographic determination of their composition.

There is apparently an incompatibility between high temperature tantalum and liquid cesium, however, this incompatibility may not exist or may be less pronounced if the cesium is in the vapor state. An electrically heated flash evaporator will be installed between the positive displacement feeder and the tunnel so as to vaporize and superheat the cesium before it enters the tunnel.

IX. Cesium Feed and Bleed Apparatus Test

A. Summary

An experiment designed to check out the principles of operation of the cesium feed and bleed apparatus for the closed loop MHD machine was carried out. Operation of both the feed and bleed apparatus was generally successful but showed the need for some improvements. Development work in the immediate future will be done on the bleed apparatus since the evaporator feed apparatus used in this experiment is now regarded as a backup to the positive displacement feeder.

B. Description of Operation

The feed and bleed systems together control the pressure level and the cesium atom concentration in the closed loop plasma. Cesium is introduced by the feed system in which a flow of helium, about .1% of the loop circulating flow or 6.75×10^{-5} kg/sec, metered by a critical flow orifice, is bubbled through a heated bath of cesium metal and thence to the loop. The temperature of the bath determines the vapor pressure of the cesium and hence the cesium atom concentration in the cesium saturated helium leaving the bath. A flow of loop gases equal to the feed flow plus other additions for cooling gages, etc. is bled from the loop through the bleed system. Therein the gases are cooled and divested of their cesium vapor by contact with water. The cesium

atom concentration in the bleed gases is deduced from the gas flow, water flow and CsOH concentration in the water as determined by electrical conductivity.

In the closed loop MHD machine the feed and bleed systems are connected to separate points in the vicinity of the motor inlet. In this experiment the feed system was directly connected to the bleed system and some of the auxiliary apparatus planned for the closed loop system was omitted. The cesium-helium feed and bleed experimental setup is as shown on Figures 6 and 7. Referring to Figure 7 the electrical controls are mounted on the panel at the extreme right of the picture. The cesium metal containing apparatus and the measuring burets are located under the hood which is enclosed by 1/2" transite panels during operation. The scrubber and main collector are in front of the hood. Helium and water valving manifolds and line heater control are to the left of the hood and gas metering equipment is at the extreme left. The cesium supply bottle is beneath the bench. Water and helium are brought by overhead lines from water conditioning equipment and gas bottles not shown. The bucket on the floor acts as a sump for the water from the outlet of the scrubber and water is lifted from the bucket to the sink by a centrifugal pump.

Operation of the experimental system is as follows. The cesium is piped into the system from a bottle, and after purging all possible paths in both the feed and bleed system with helium, the

communicating valve is opened and a telescoping tube is lowered into the bottle. Cesium is then driven into the evaporator via V8 and V2 by helium controlled at 5 psig by the pressure reducing valve. When the cesium reaches the high contact in the evaporator, the relay is energized and V2 is deenergized thereby closing and stopping the cesium flow. When the cesium level goes below the lower contact due to evaporation, the relay is deenergized and V2 is energized to open position. Thus the cesium level is maintained between the upper and lower contacts.

Cesium temperature in the evaporator is maintained by a recorder-controller which controls the evaporator heater. The walls of the tube connecting the evaporator to the scrubber are maintained at a temperature above the dew point of the cesium by a line heater.

A large quantity of cesium is needed in starting up the loop. This is supplied by energizing V1 thus bypassing the critical flow orifice and admitting a large amount of helium to the evaporator, violently agitating the bath, and causing cesium to "slop over" into the outlet tube.

The scrubber is supplied with 1 gpm flow of either deionized or softened water, which enters the scrubber tangentially and coats the wall of the vertical tube. Downstream of the scrubber, water can be diverted either into the main collector or to the sump by energizing or deenergizing normally closed V15 and normally open V21. In normal operation softened water is run through the scrubber but

diverted from the main collector. Prior to a sample period the scrubber supply is switched to deionized water and when the deionized water conductivity cell shows .2 μ mho/cm or lower, indicating that all soft water is flushed out, the flow is switched to the main collector for a measured period during which total gas flow is metered by a wet test meter and by a domestic type gas meter.

A water sample from the main collector is driven into the 100 ml buret by helium admitted to the collector via V20. This sample is run into the sample conductivity cell and diluted with deionized water previously admitted to the 250 ml buret via V19.

The concentration of cesium atoms in the helium flow can be calculated as follows.

$$\% \text{ cesium atoms} = \frac{\text{gm-mols total cesium flow}}{\text{gm-mols total helium flow}} \times 100 = \frac{M_c}{M_h} \times 100 \qquad (3)$$

where

$$M_h = \frac{\text{Total helium weight flow } (W_h)}{\text{Molecular weight of helium}} = \frac{W_h}{4} \qquad (4)$$

and $$W_h = \frac{P_h V_h}{R_h T_h}$$

(P_h, V_h, T_h and R_h are respectively pressure, total volume, and temperature of helium at the meter and gas constant for helium),

$$M_c = \frac{1}{1000} V_w C_w = \frac{1}{1000} V_w C_x \left(1 + \frac{V_d}{V_S}\right) \quad (5)$$

$$= \frac{1}{1000} V_w \frac{L}{1000 \Lambda} \left(1 + \frac{V_d}{V_S}\right) \quad (6)$$

V_w, C_w, C_x, V_S, V_d, L and Λ are respectively water total volume flow, measured concentration of CsOH in water and diluted water sample ($\frac{\text{mols}}{\text{liter}}$), volume of sample (ml), volume of sample diluent water (ml), measured conductivity of diluted water sample (μ mhos/cm), and computed conductivity of CsOH solution (mho-cm^2/mol).

Conductivity (Λ) can be read directly from Figure 8 if infinite dilution is assumed. This assumption results in less than 1% error for samples diluted to 100 μ mhos/cm or less which is full scale for the instrument.

The cesium atom concentration can be computed from the temperature of the cesium bath and the cesium flow also. Thus, on the assumption that the cesium vapor behaves as a perfect gas and that the vapor leaving the bath is saturated:

$$\frac{\text{Mass of cesium in He-Cs mixture}}{\text{Mass of helium in He-Cs mixture}} = \frac{P_c}{P_h} \times \frac{m_c}{m_h} = \frac{M_c}{M_h} \times \frac{m_c}{m_h}$$

or: $$\frac{M_c}{M_h} = \frac{P_c}{P_h}$$

(m_c and m_h are respectively the molecular weights of cesium and helium). Vapor pressure (P_c) vs. temperature for cesium can be read from Figure 9.

At the conclusion of the test the cesium remaining in the evaporator after the experiment is driven back to the supply bottle by closing V16 and V15 via the salvage valve and V8. The helium displaced from the bottle is bubbled into the cesium disposal sump via V5.

The experimental system included some of the safety features planned for the closed loop system, for instance, a power failure interrupts the flow of cesium to the sump by closing V2 and switches the water flow direct to the water sump by closing V15 and opening V21. Also the cesium in the evaporator can be dumped under helium cover to the kerosene sump by manually releasing a spring loaded punch against a thin diaphragm.

C. Test Procedure and Results

Initially the evaporator was filled only to the lower contact and the cesium saturated vapor was directed to the water filled main collector without any water flow. The evaporator was heated to 400°C. In this mode occasional popping sounds which increased in frequency when

the "inch" button was held down for 10 seconds indicated that droplets of cesium were reacting explosively with the water in the main collector. Pinging sounds were heard when the water flow was started and directed to the water sump. These effects are probably due to condensation of cesium in the unheated 3" of vertical line above the scrubber.

The combined helium and water flow produced a 2 psi drop across the scrubber. Since friction pressure drops are computed to be very much lower than this it is believed the scrubber operates nearly full of water. Since the pressure drops were lower in the glass model tests which were previously performed, it is assumed that the additional pressure drop is due to the constriction in valve V15 which was not in the model tests.

It was noted that after trying the inch button the "high cesium" light went on and stayed on indicating that the insulators for the high and low cesium contacts were wetted by the cesium.

There was a certain amount of white irritating vapor released from the water sump indicating that not all of the cesium was removed in the scrubber. However no alkalinity was detected in the wet test meter bath. It is probable that no cesium gets by the main collector when the helium is bubbled through it after passing through the scrubber.

Analysis of test results, made by bubbling a measured amount of cesium-helium mixture through a known amount of water in the main collector, yielded a 1.74% cesium atom concentration by the cesium vapor pressure method and 2.43% by CsOH concentration in the water.

Improvement in technique is obviously necessary to give more assurance of the seeding concentration measurement. Improvements needed are better cesium bath temperature control and better sampling procedure.

Because of the wetting of the insulator around the "high cesium" indicator contact, the automatic level control feature of the feeder was not tried. However solenoid V2 is capable of controlling the flow of cesium and well adapted to the intended purpose and there is no reason to believe that this feature is not workable if the wetting of the contact insulators can be remedied. It is believed that this can be readily accomplished by local heating of the insulator contacts.

A preliminary test prior to the run showed that the 10 micron filter in the cesium salvage line had inadequate flow capacity. This filter was eliminated prior to the run.

Continuous recording of the cesium metal temperature showed that the cesium bath could be controlled to within $\pm$ 5°C of the desired temperature. More accurate temperature control may be needed to give adequate control of the cesium atom concentration because cesium vapor pressure is extremely temperature dependent.

The water conditioning equipment functioned adequately, the deionizer held conductivity below .2 micro mho/cm at 1 gpm flow and the hardness measured as $CaCO_3$ at the softener outlet was too low to be detectable by the AZO dye method. One charge of deionizing resin was depleted in the test. The reasons for this rapid depletion are being sought.

The domestic type gas meter, Rockwell Manufacturing Company No. 310, gave readings within ± .5% of those obtained from the wet test meter but only if an integral number of revolution of the fast pointers on both meters was timed.

D. Conclusions

1) The evaporator feeder is a satisfactory system if the wetting of contact insulators is remedied. More accurate temperature control is needed.

2) The basic principle of the bleed apparatus is satisfactory but the flow resistance through the system should be reduced to avoid excessive back pressure in the closed loop MHD machine.

3) The operating procedure and sampling method for the bleed apparatus is cumbersome and the apparatus should be revised to remedy this condition.

E. Recommendations

1) Concern over the hazard of the approximately 1.3 lb of cesium at 500°C in the evaporator and the experimental evidence from 3/4" tunnel tests that conductivity of the plasma does not rapidly change when seeding is interrupted has led to the decision to use the existing positive displacement apparatus to seed the closed loop MHD machine. Development of the evaporator feeder should therefore be discontinued for the immediate future. It should be remembered

that this apparatus is available and could be used with only a small amount of development.

2) The bleed system should be panel mounted and revised so that in normal operation the bleed helium has only a single path through the apparatus, with no need for disassembly and cleaning of parts during sampling.

3) The positive displacement feed system should be revised to permit repeated filling of the cylinder and transfer of 15 lb of cesium to a single container so that enough cesium can be stored in the apparatus to carry out a 50 hour test. A heater should be installed downstream of the cesium valve to insure that all cesium is vaporized before it enters the loop.

4) When alterations 2 and 3 are complete the 3/4" tunnel should be run to check out the revised positive displacement feed apparatus and techniques and to perform a controlled experiment to determine the effect of cesium on tantalum under tunnel conditions. Following this run the revised bleed system should be direct connected to the feed system outlet and a combined run should be made to rigorously check out the accuracy of measurement of cesium atom concentrations.

5) As a future improvement the system should be revised to permit continuous monitoring of water conductivity, water flow and helium flow in order to simplify measurements of percent cesium atoms.

6) In future tests the helium and water flows away from the bleed system should be observed for evidence of alkalinity to evaluate the effectiveness of cesium removal.

X. Motor Section Power Supply

Tests were run to evaluate the complete motor power supply under simulated operating conditions. It was found that the circuits performed satisfactorily and were easily controlled. All circuits were loaded to approximately 20 amperes, the maximum allowable current, and the voltage averaged about 180 volts. This represents a total power output of 72 KW from the 20 circuits of the power supply. Since all of the components ran without overheating, apparently there will be no cooling problem during future operation.

It was found that the output voltage of any particular pair of terminals on the power supply was not significantly altered by the loading on the other circuits.

At the maximum setting of the powerstats which are used to control the motor power, it was found that the output voltage was 203 V while the output circuits were loaded to their maximum rating of 20 amps. Based on the original design a maximum voltage of 175 V under loaded conditions was required. The additional 28 V will provide a safety factor in starting the loop. Figure 10 shows the effect of powerstat setting and current flow on the output voltage.

XI. Motor and Generator Magnets

Both magnets have been assembled and installed in their operating positions, as shown in Figure 11. Pole piece extensions have been added to

improve the uniformity of the magnetic field, and Figure 12 is a magnetization curve for this new pole piece arrangement. Note that the required flux density of 1.7 webers/sq meter is achieved at a current of 635 amperes, and that a current overload of 10 percent produces a flux density of 1.78 webers/sq meter.

The three current regulators have been built and debugged, one of which will be used to control an end return heater and the other two will operate the magnets. Detailed schematic drawings are shown in Figure 13, 14, and 15, regulator No. 1 differing from the others only in the wiring arrangement of the variac motor. The current regulator was used to operate the motor section magnet while obtaining the data for the magnetization curve and field mapping. The performance curve appears in Figure 16. At the operating point of 1.7 webers/sq meter, the regulator can maintain the set value within $\pm$ 1.2 percent.

The working volume of the magnet was mapped with the pole piece extensions bolted into place. The results are shown in Figures 17, 18, and 19. Along the centerline, the flux density drops 5.9 percent from the center to the ends of the motor section. In the horizontal and vertical directions the maximum deviation at a flux density of 1.7 webers/sq meter is $^{+\ 1\%}_{-\ 9\%}$. This is a considerable improvement over the maximum deviation of 20 percent reported in Interim Report No. 3 for the same magnet without the pole piece extensions.

XII. Some Generator Losses

A. Electrode Circulating Current Power Loss

Whenever the ratio of the electron cyclotron frequency to the effective collision frequency, $\omega\tau$, is not small, transverse currents in an MHD generator produce axial (Hall) voltage gradients. If the generator has continuous electrodes the axial voltage gradient causes axial current to flow resulting in a power loss. One way to reduce this loss is to have many pairs of electrodes with insulation between each pair (otherwise known as segmented electrodes) reducing the axial current. In order to make this loss of power zero an infinite number of electrodes per unit of axial length are required, a practical impossibility. With a finite size of electrode there are small axial currents associated with each electrode pair which represent a power loss.

The current distribution in an MHD generator with conductivity a tensor quantity was studied by Hurwitz et al.[4] The results of the study were used by Dzung[5] to investigate power losses associated with finite electrode spacing and with circulating currents at the duct ends.

---

4) H. Hurwitz, Jr., R. W. Kilb, and G. W. Sutton, "Influence of Tensor Conductivity on Current Distribution in a MHD Generator," Journal of Applied Physics, Vol. 32, Number 2, February 1961, pp. 205-216.

5) L. S. Dzung, "The Magnetohydrodynamic Generator with Hall Effect at the Duct Ends," The Brown Boveri Review, Volume 49, No. 6, June 1962, pp. 211-225.

Dzung proposed a power reduction factor, r, which is

$$r = \frac{1 + \gamma\beta^2}{1 + \beta^2} \tag{7}$$

where γ is the compensation factor for Hall current ($\gamma = 0$ for continuous electrodes, $\gamma = 1$ for infinitely segmented electrodes) and β is the product $\omega\tau$. An alternate expression for β is

$$\beta = \omega\tau = \mu B \tag{8}$$

where μ is the electron mobility (sq m/weber) and B is the magnetic flux density in webers/sq m. This power reduction factor can be incorporated into an effective conductivity σ'_e which is

$$\sigma'_e = r\,\bar{\sigma}'_g = \left(\frac{1 + \gamma\beta^2}{1 + \beta^2}\right)\bar{\sigma}'_g \tag{9}$$

where $\bar{\sigma}'_g$ is the magnitude of the gas conductivity. The compensation factor γ is a function of β and the electrode spacing ($2\rho d$) where ρ is the spacing parameter. The electrode spacing in the generator is

$$2\rho d = 1.0 \text{ in.} = 0.0254 \text{ m}$$

resulting in

$$\rho = 0.182 \quad .$$

The value for β in the working fluid He + 0.015 Cs (Interim Report No. 2) is

$$\beta = 1.568 \quad .$$

Using the values for ρ, β and Figure 5 of Dzung's paper we get a value for γ of

$$\gamma = 0.685$$

The power reduction factor r is now

$$r = 0.775 \quad .$$

In other words the closed loop generator will produce only 77.5 percent of the power theoretically attainable with infinitely segmented electrodes. The effective conductivity σ'_e using the value in Interim Report No. 2 for $\bar{\sigma}'_g$ and equation (9) is

$$\sigma'_e = r\ \bar{\sigma}'_g = 0.775\ (14.54) = 11.27\ \frac{\text{mho}}{\text{m}} \qquad (10)$$

The power reduction factor, r, must be applied in addition to that for end return leakage current losses which will be discussed below.

B. End Eddy Current Power Loss

Dzung[5] investigated power loss in an MHD apparatus from circulating currents at the ends, where the circulating currents are the result of a decrease in the magnetic flux density, B. He treated the extreme case of B = 0 everywhere outside of the generator.

This is not true for our generator, rather the flux density continues for a significant distance from the end electrodes, especially with the addition of the pole piece extensions discussed earlier in this report. Therefore, the end eddy current power loss will be neglected at this point, but an effort will be made to evaluate its contribution, if any, experimentally.

C. End Return Leakage Current Power Loss

The transverse currents in the closed loop generator will produce an axial (Hall) voltage gradient. Because both tantalum end returns are grounded, a leakage current, I_L, will flow out of one end of the generator, into the tantalum end return through ground, out of the other end return and back into the other end of the generator. This axial voltage gradient and the resulting leakage current are illustrated in Figure 20.

In Interim Report No. 2 this power loss was calculated using the electrical leakage factor, C, which was

$$C = \frac{L_T}{\beta^2 L + L_T} = 0.504 \quad .$$

This means that the closed loop generator will produce only 50.4 percent of the power theoretically attainable with infinitely segmented electrodes.

This end return power loss is particularly objectionable because it is a characteristic of this particular apparatus rather than of MHD generators in general. For instance a greater separation between the generator and the end returns would reduce this loss. If the end returns were constructed of an insulating material this loss would disappear.

Steps have been taken to eliminate this loss by the insertion of guard electrodes between the ends of the generator and the grounded end returns. The guard electrodes are discussed later in this report.

D. Numerical Values of the Two Losses

The generator output power, P_{gi} (ideal) assuming an infinite segmentation of the electrodes and no end return power losses would be:

$$P_{gi} = \bar{\sigma}_g U_g^2 B^2 L A_g \eta_g (1 - \eta_g) \qquad (10)$$

where the symbols are as defined in Interim Report No. 2. The values for these symbols, assuming V_m = 175 volts, U_m = 425 m/sec and η_g = 0.6, are

$$\bar{\sigma}_g = 14.54 \text{ mho/m}$$
$$U_g = 472 \text{ m/sec}$$
$$B = 1.7 \text{ webers/m}^2$$
$$L = 0.4 \text{ m}$$
$$A_g = 0.00389 \text{ m}^2$$

Substituting these values into equation (10) gives

$$P_{gi} = 3.49 \text{ kilowatts}$$

The corresponding equation including the two losses discussed above is

$$P_g = \bar{\sigma}_g U_g^2 B^2 L A_g \eta_g (1 - \eta_g) r C \qquad (11)$$

Substituting the values from equation (10) along with the values for r and C gives for the power P_g:

$$P_g = 1.36 \text{ kilowatts}$$

The guard electrodes by eliminating the end return leakage current will increase the power output, P_{gg} (guard electrode), to

$$P_{gg} = 2.70 \text{ kilowatts}$$

XIII. Hall Voltage Guard Electrodes

The guard electrodes decrease power loss and permit one to analyze the operation of the generator as a segmented Faraday device. These electrodes prevent axial Hall currents from flowing from the end electrodes to the tantalum liner (end return). These electrodes are located approximately half way between the end electrodes of the generator and the beginning of the tantalum liner (see Figure 2).

Each electrode consists of a rectangular piece of tantalum imbedded in the bricks so that it is flush with the four walls of the duct. The guard electrodes are maintained at a potential so that the voltage gradient along the center line of the duct between the guard electrodes and adjacent generator end electrodes is zero; therefore, the current along the center line is zero. Provisions have been made to increase the temperature of a portion of the guard electrodes so that their current is not limited by thermionic emission.

Each pair of probes near the guard electrodes (labeled voltage probes in Figure 21 and velocity probes in Figure 2) serve two purposes.

The first purpose is to sense the axial voltage gradient which must be made zero, and the second is to measure the gas velocity entering and leaving the generator. Since the probes are in a magnetic field the voltage between them is proportional to the velocity. They will be used to maintain a constant velocity in the generator duct under different loading conditions.

The region between the guard electrodes and the generator ends is an axial electric field free space. This field free space will also be used for conductivity and temperature measurements.

The guard electrode power supply schematic, shown in Figure 21, is manually controlled by two powerstats. Manual rather than automatic control was chosen for simplicity. The center line voltage gradient will be made zero by appropriate adjustments of the powerstats. The range switches permit the operator to have an increasingly sensitive measure of this voltage gradient.

The power supply outputs deliver a variable voltage from zero to 505 volts d.c. and a continuous duty current of 28 amperes. A higher output voltage can be obtained with the extra taps on the isolation transformer, and a short time current drain of 45 amperes per circuit is permissable.

One must keep in mind that the guard electrodes are necessary only because the liner (end return) is made of a conducting material, tantalum. Tantalum was used to avoid contamination of the working fluid.

DWG. 625A985

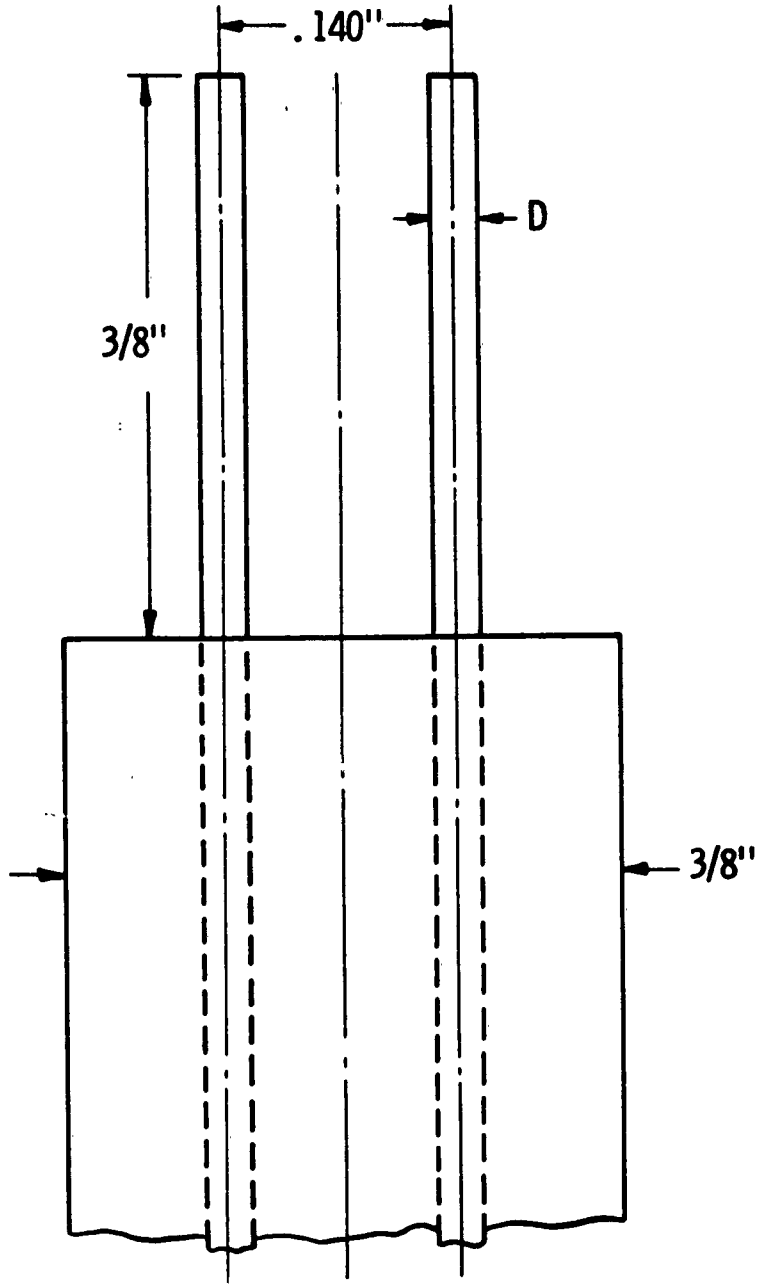

Probe #1 D = .0655 in.
Probe #2 D = .015 in.

Fig. 1 —Sketch of double probe

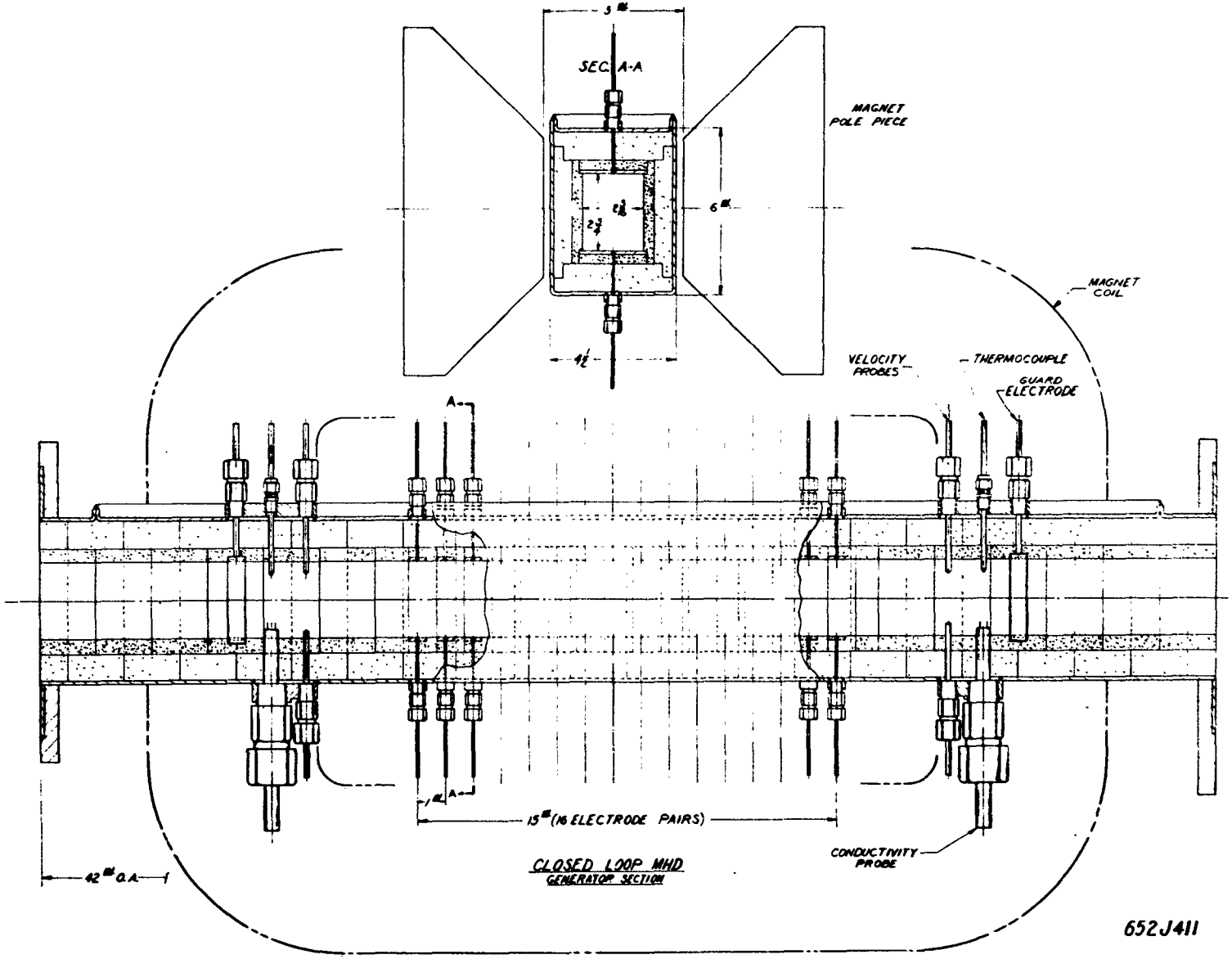

Fig. 2 - Closed Loop MHD Generator Section

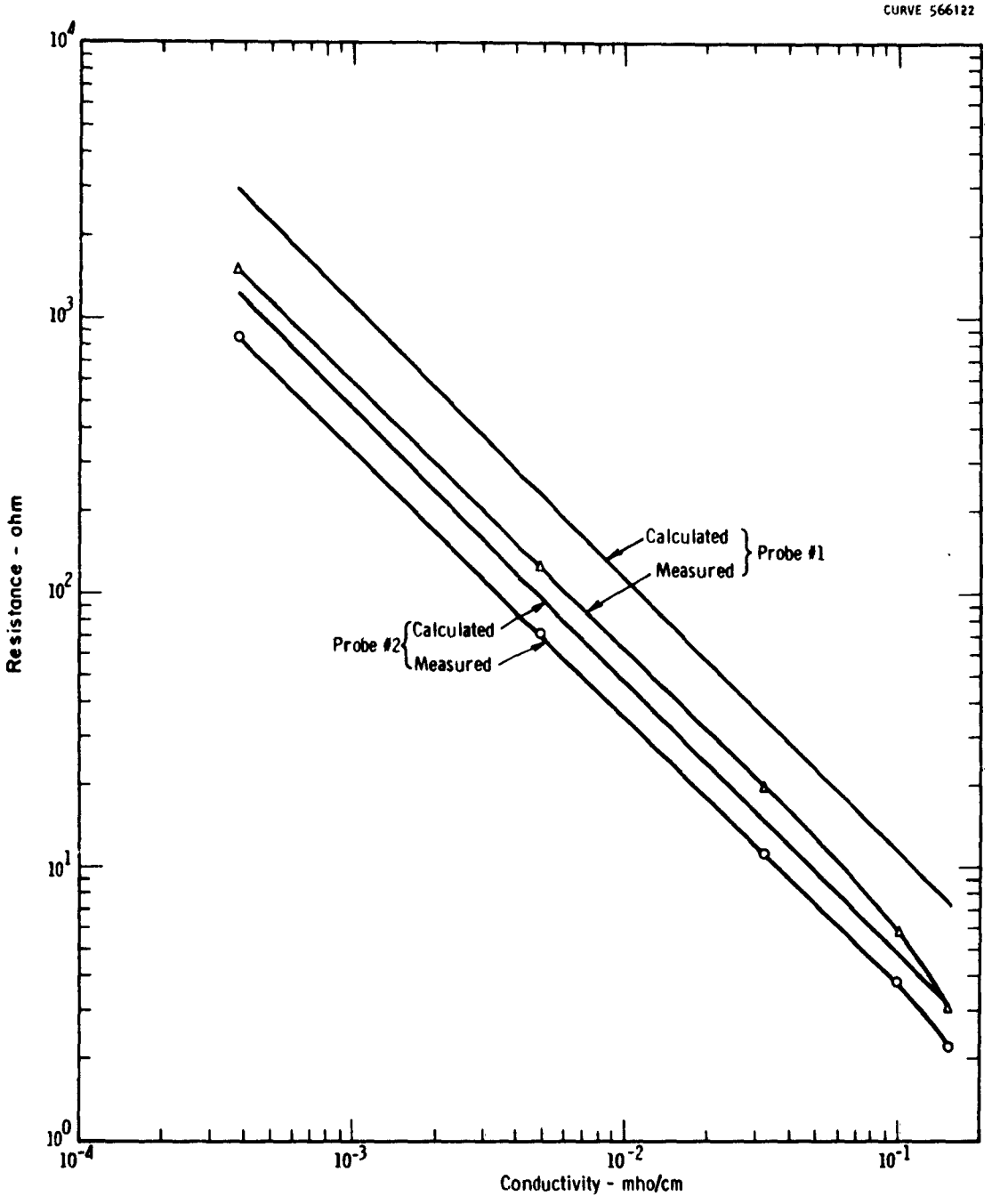

Fig. 3 –Resistance of double probe versus conductivity of KCℓ solution

DWG. 625A984

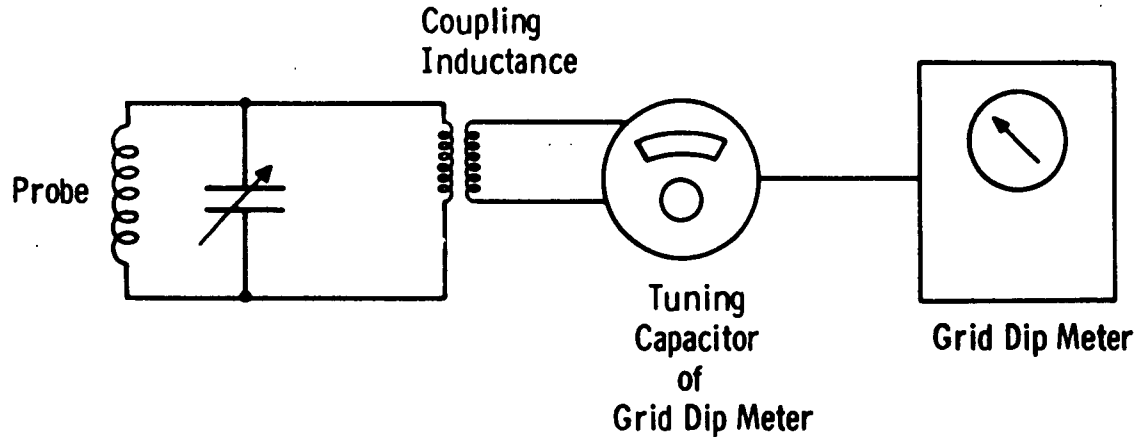

Fig. 4 —Schematic of eddy current probe measuring circuit

DWG. 625A947

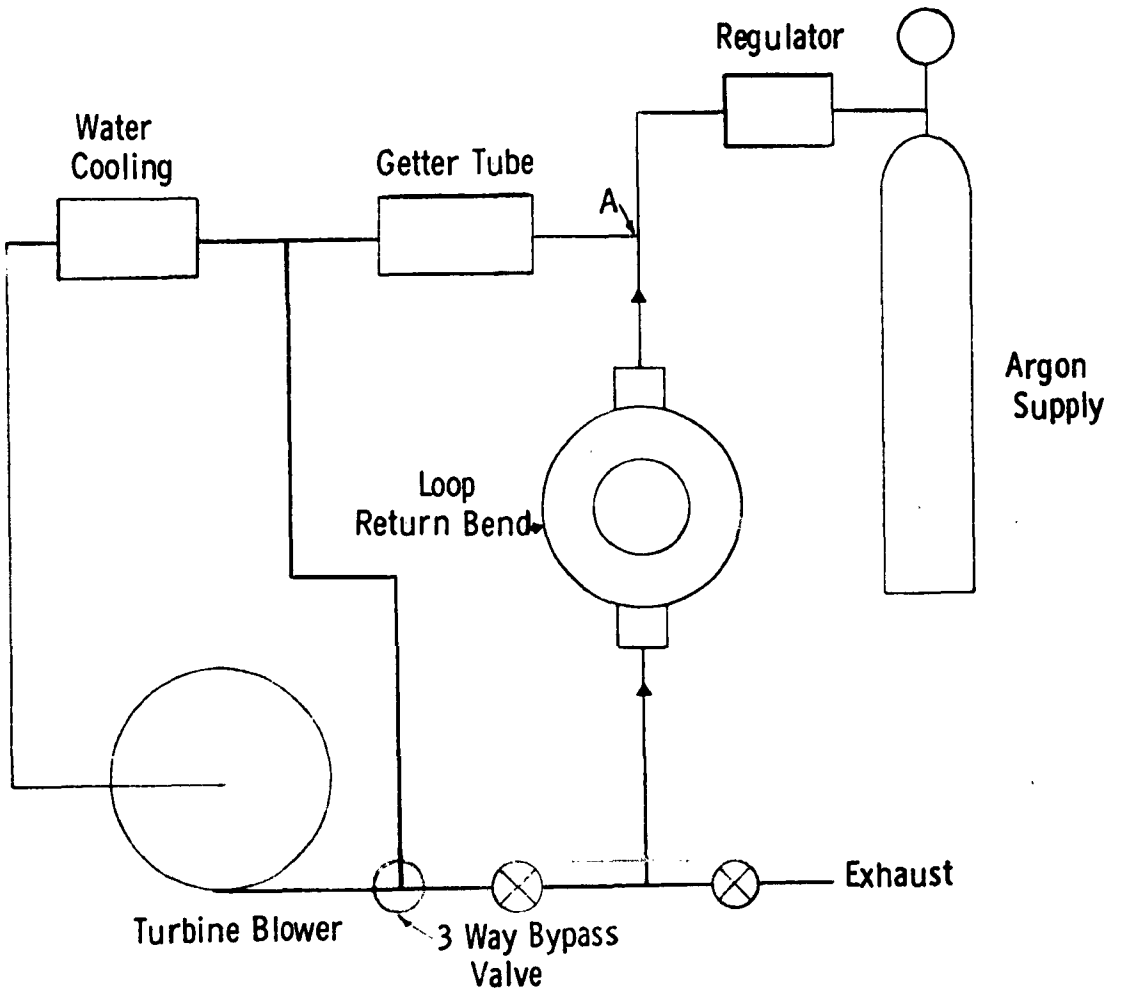

Fig. 5 - Schematic Diagram of Argon Purge and Cooling System

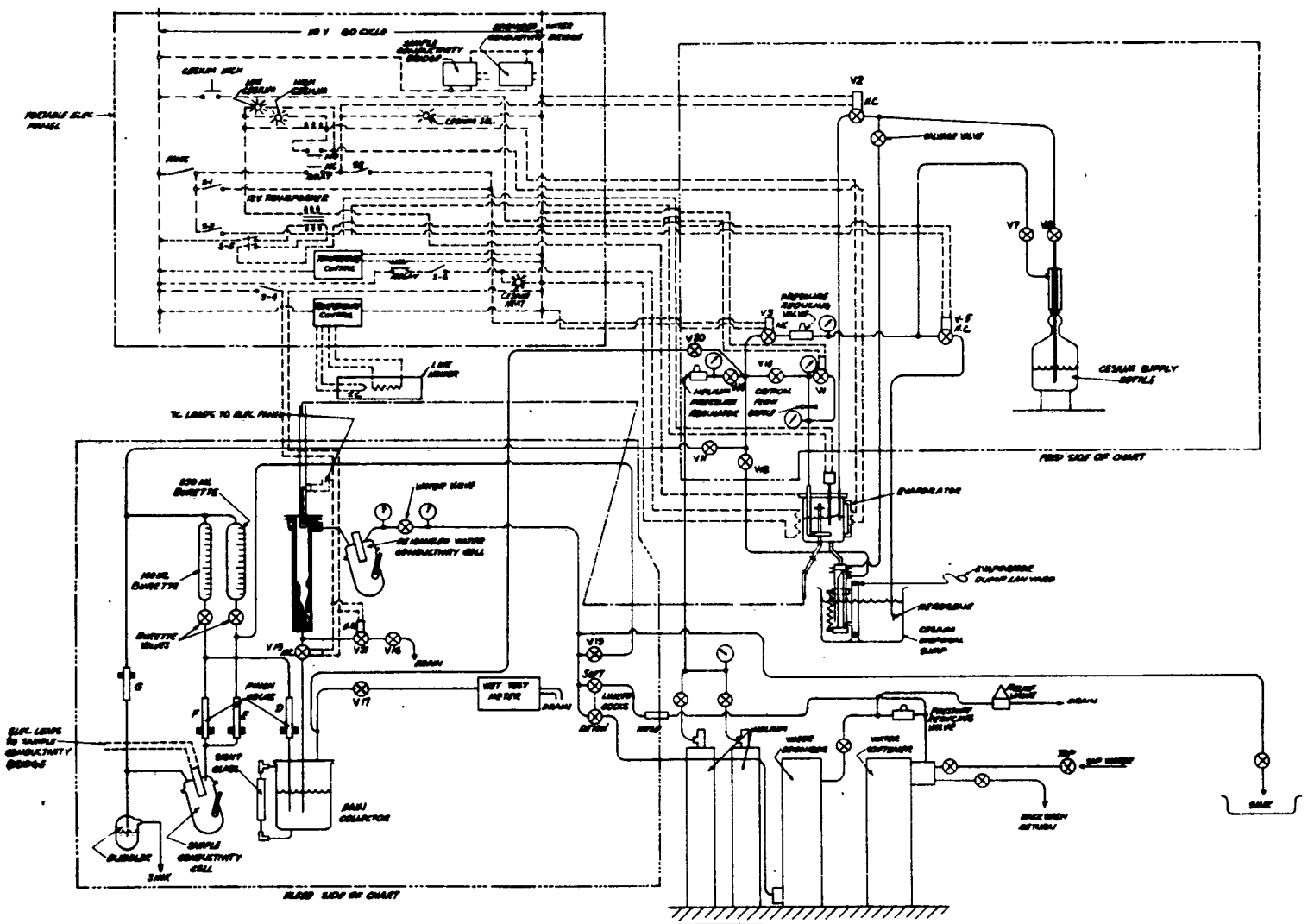

Fig. 6 - Diagrammatic Drawing of Cesium-Helium Feed and Bleed Experimental Test Setup

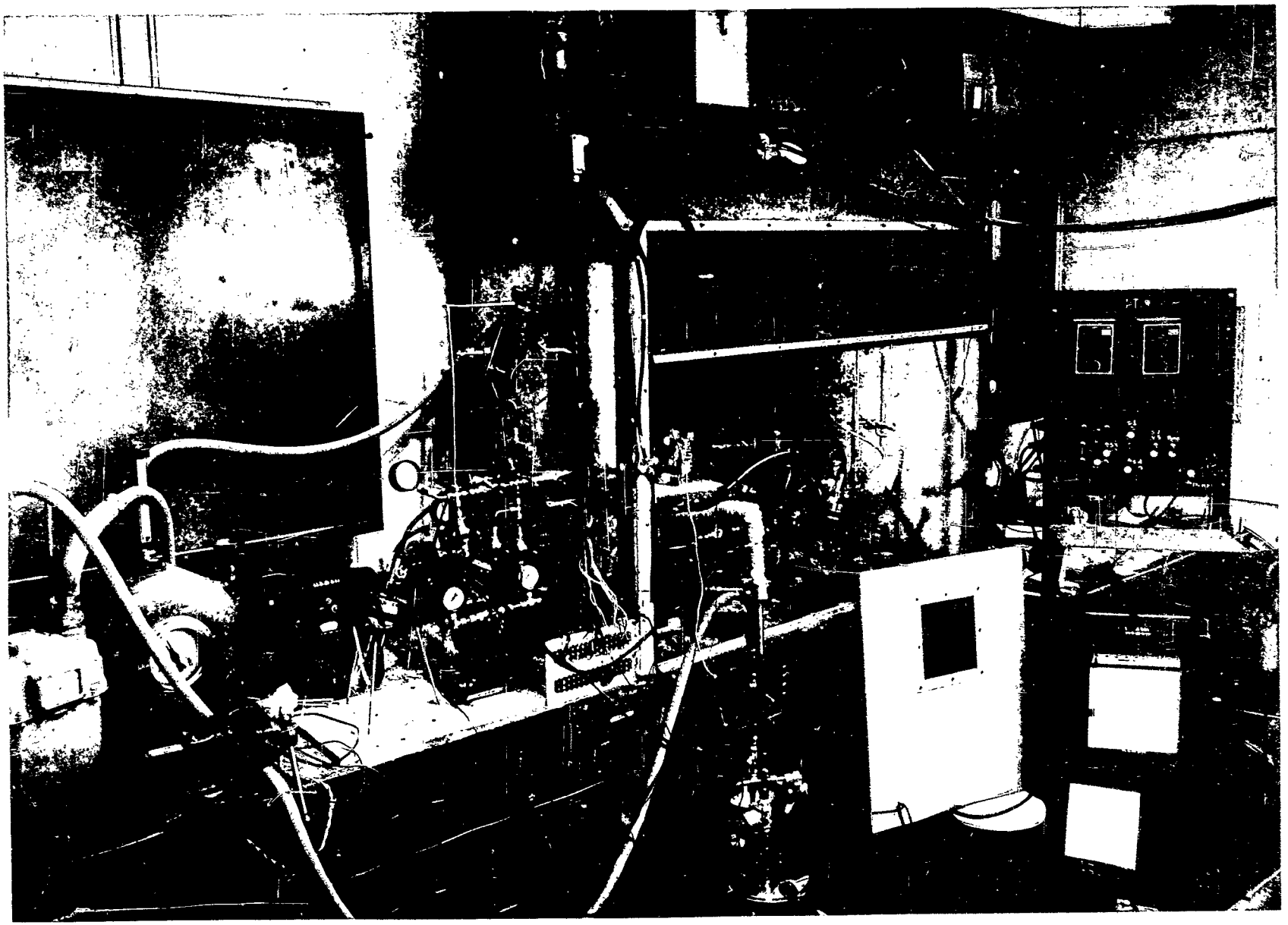

Fig. 1 - Photograph of Two-Stream Feed and Bleed Experimental Setup

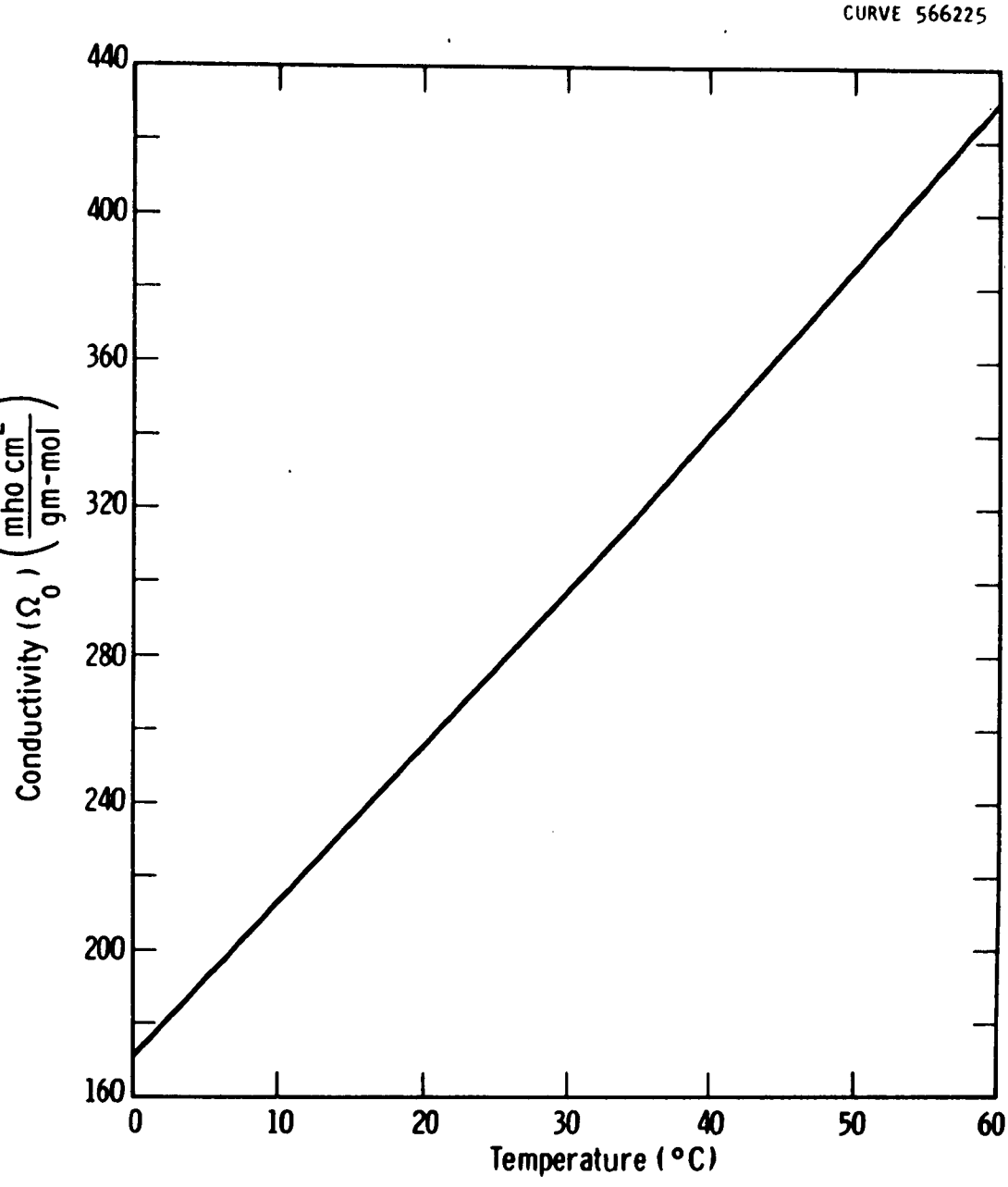

Fig. 8 - Conductivity of CsOH solution with infinite dilution

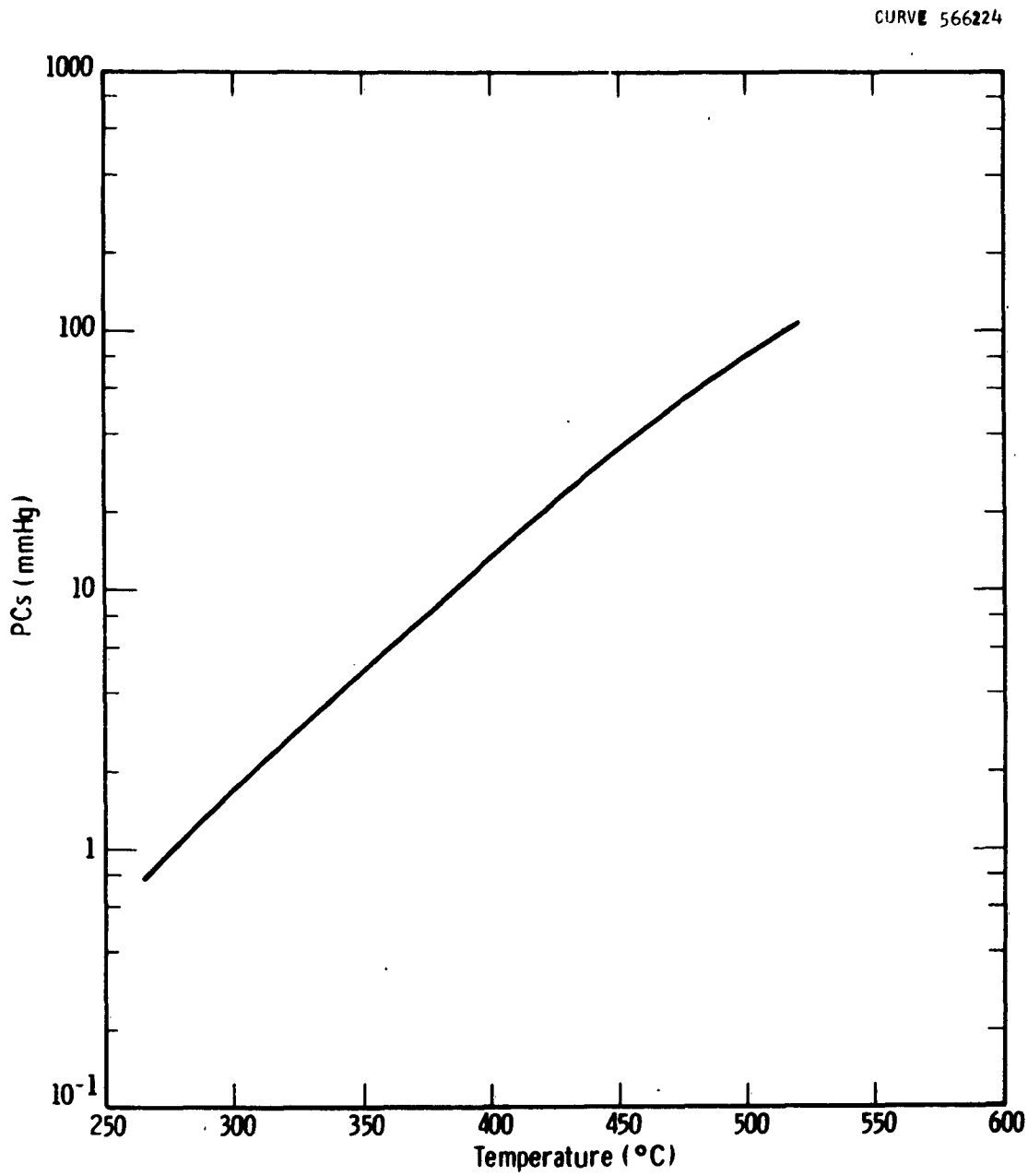

Fig. 9 - Vapor Pressure of Cesium as Function of Temperature

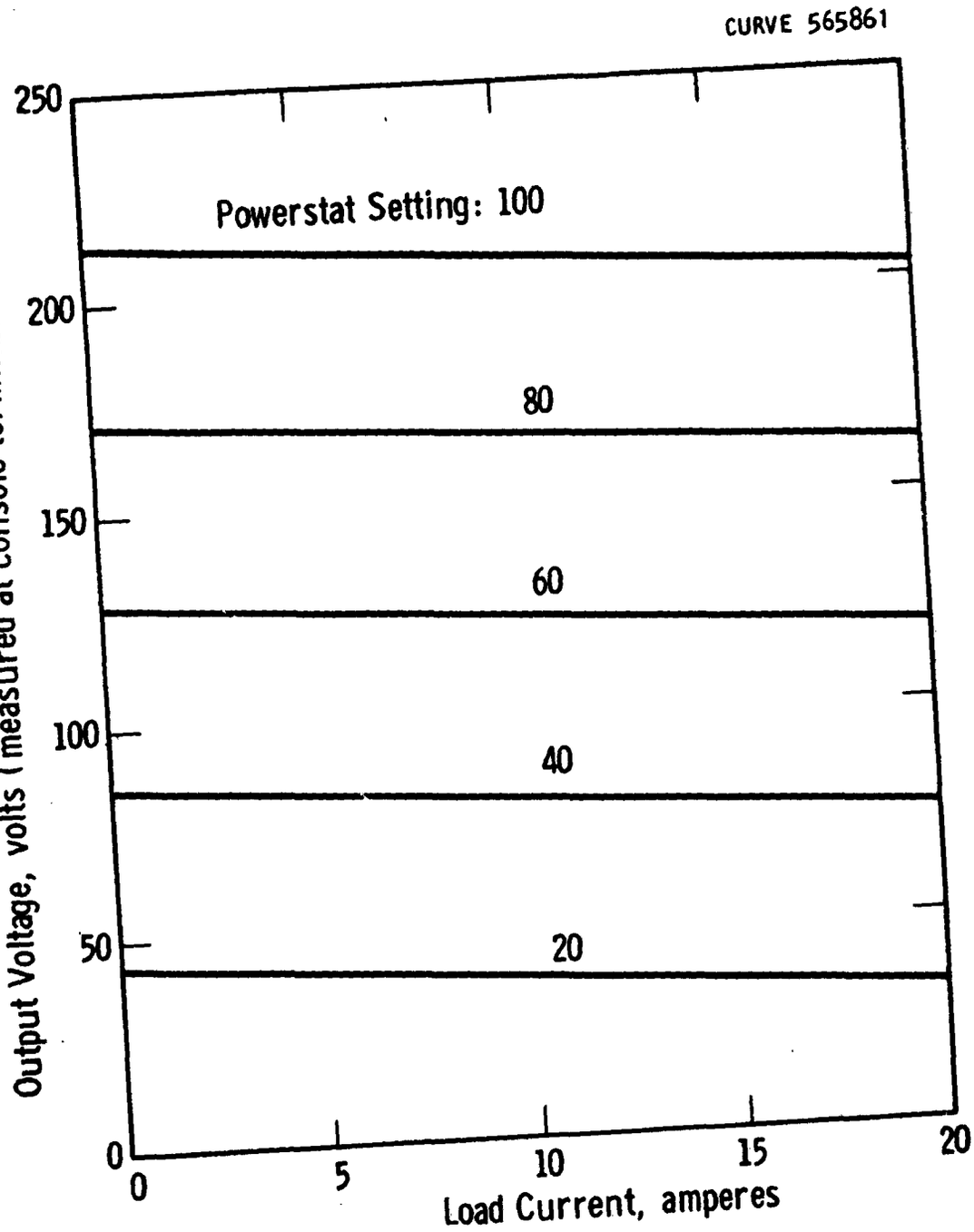

Representative loading curve motor power supply
Test run on 1/30/63

Fig. 10

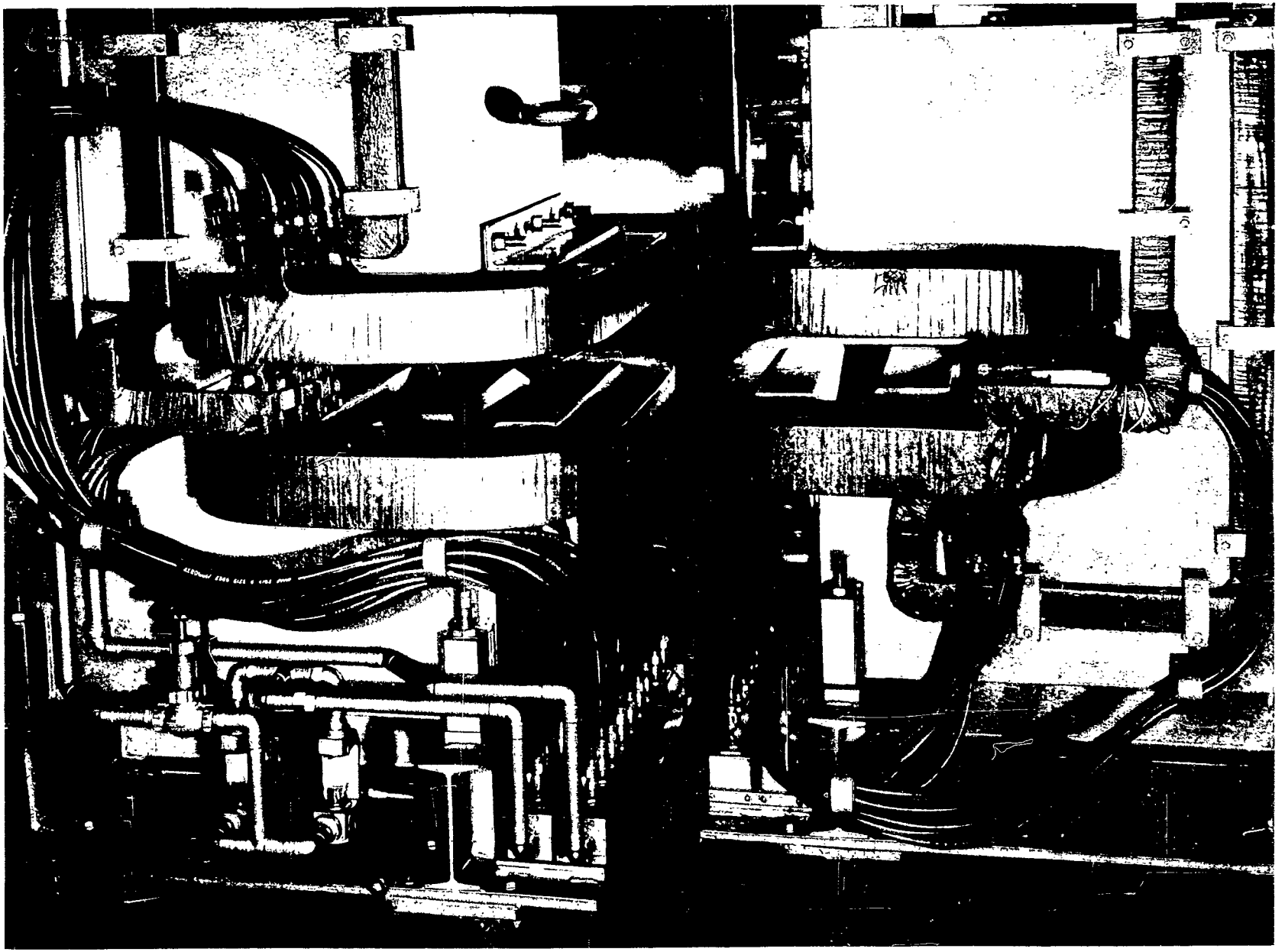

Fig. 11 - Photograph of the Placement of Motor and Generator Magnets

CLM 26258

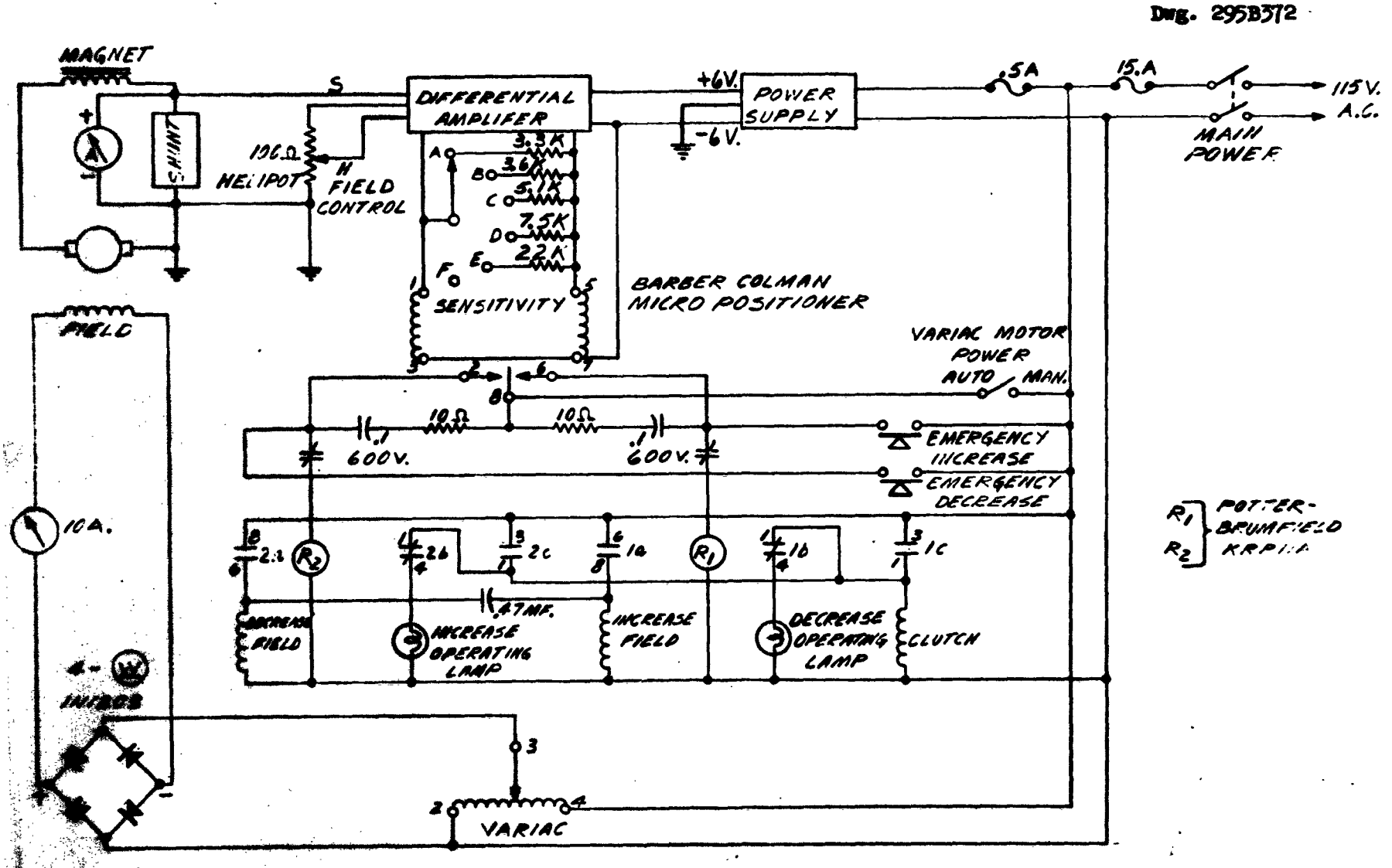

MAGNET CURRENT REGULATOR #1

Fig. 13 - Current Regulator Schematic

Dwg. 295B373

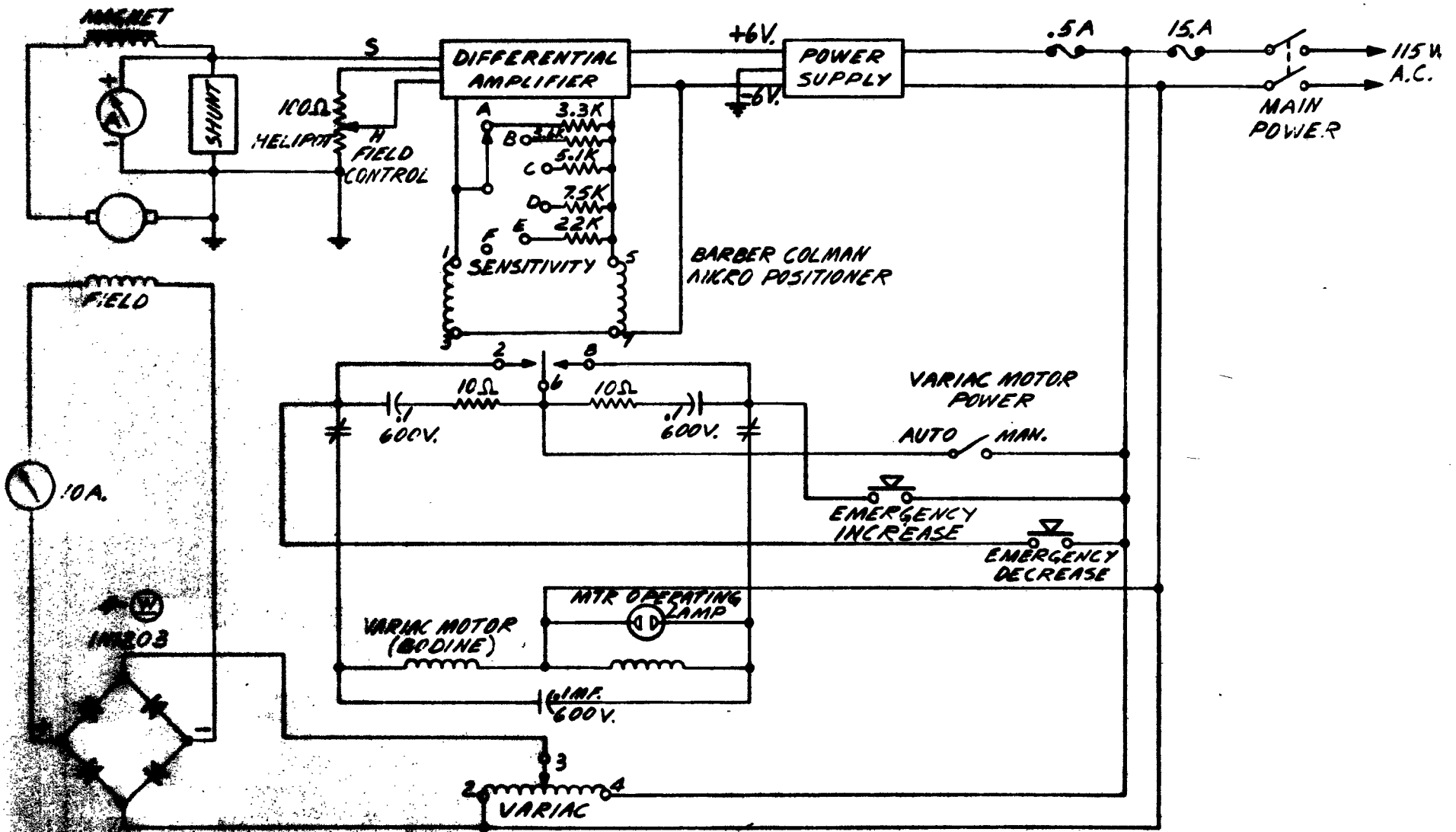

MAGNET CURRENT REGULATORS #2 AND #3

Fig. 14 - Current Regulator Schematic

Dwg. 295B371

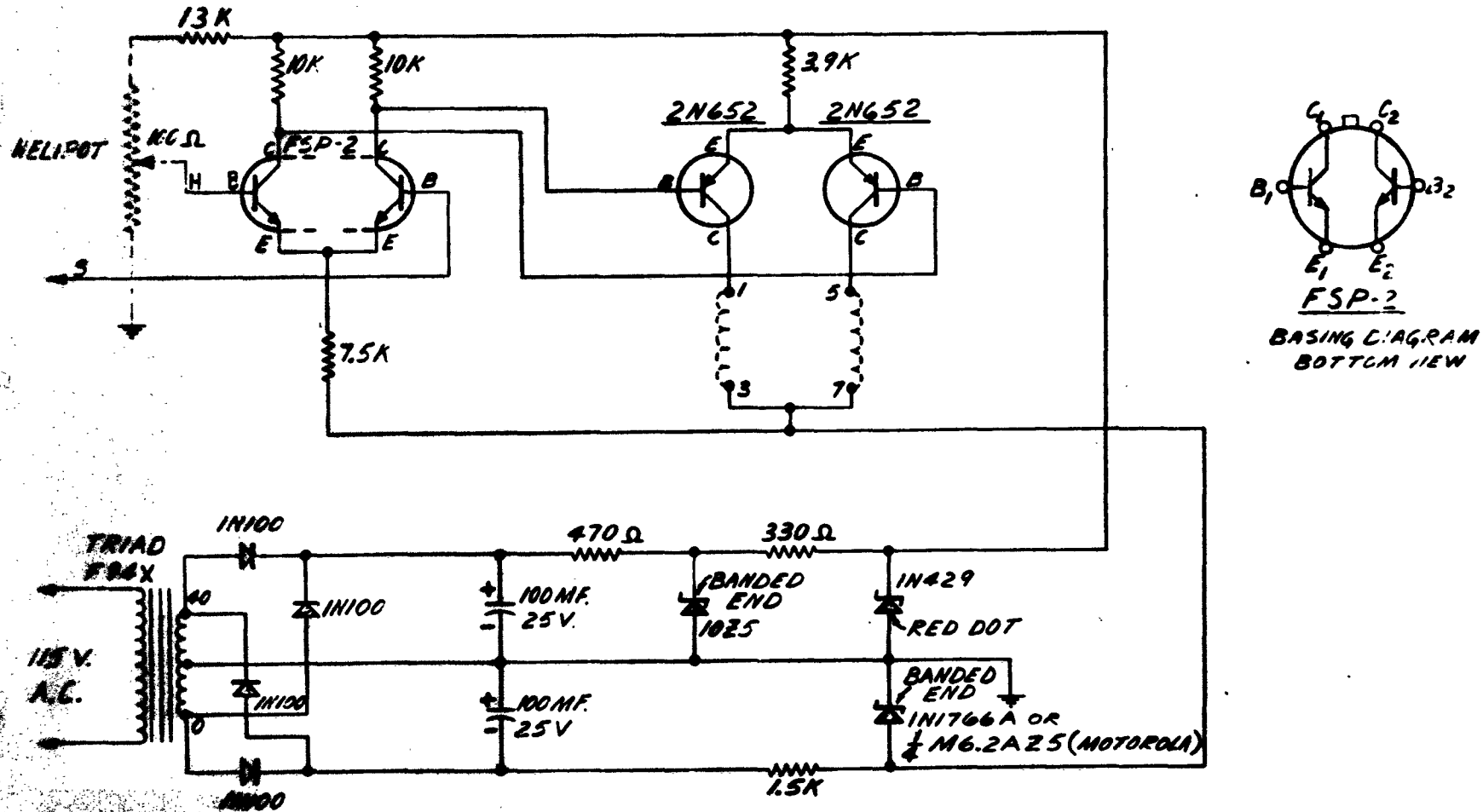

DIFFERENTIAL AMPLIFIER AND POWER SUPPLY
FOR ALL MAGNET CURRENT REGULATORS

Fig. 15 - Current Regulator Schematic

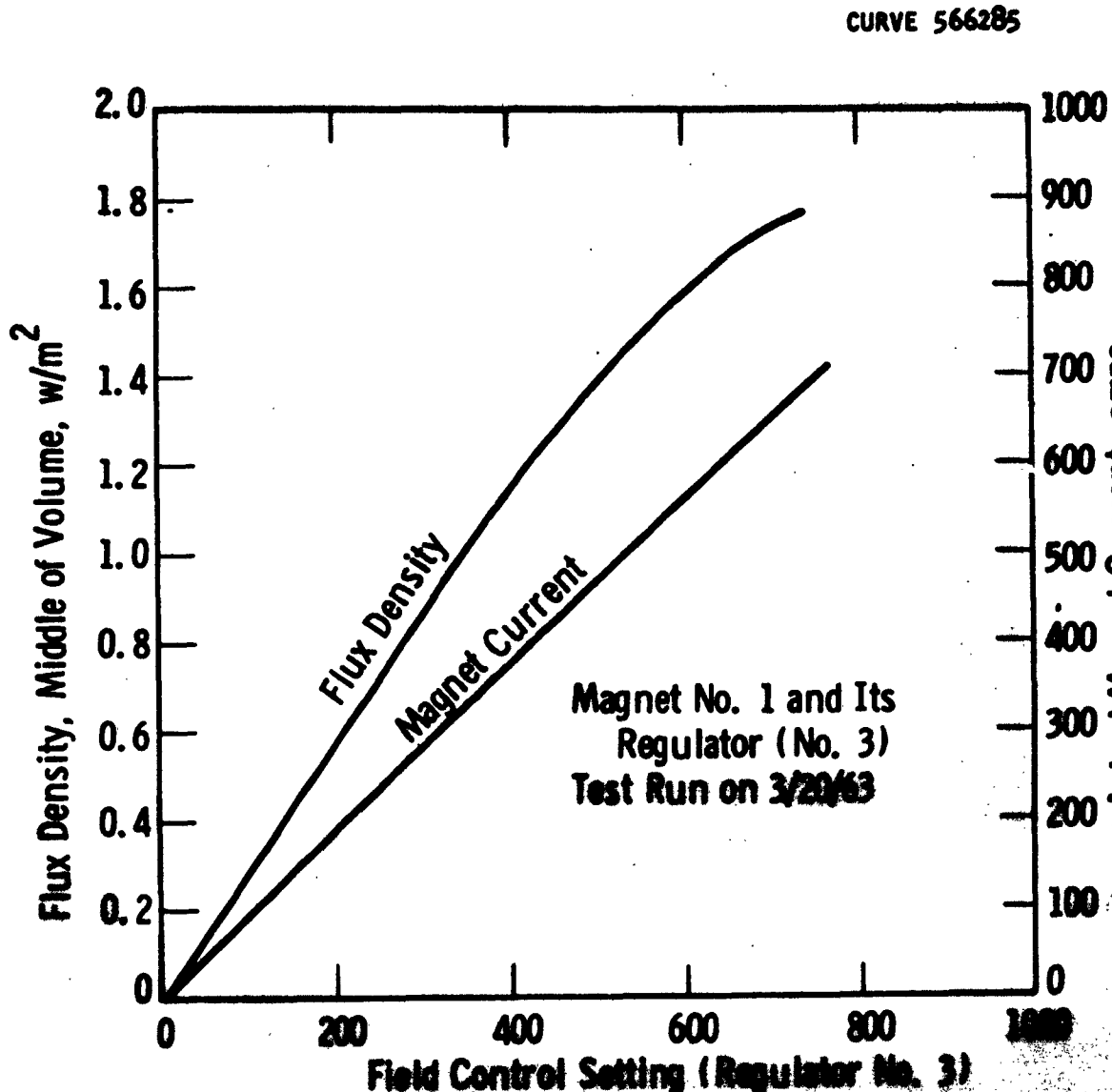

Fig. 16 - Regulator Performance Curve.

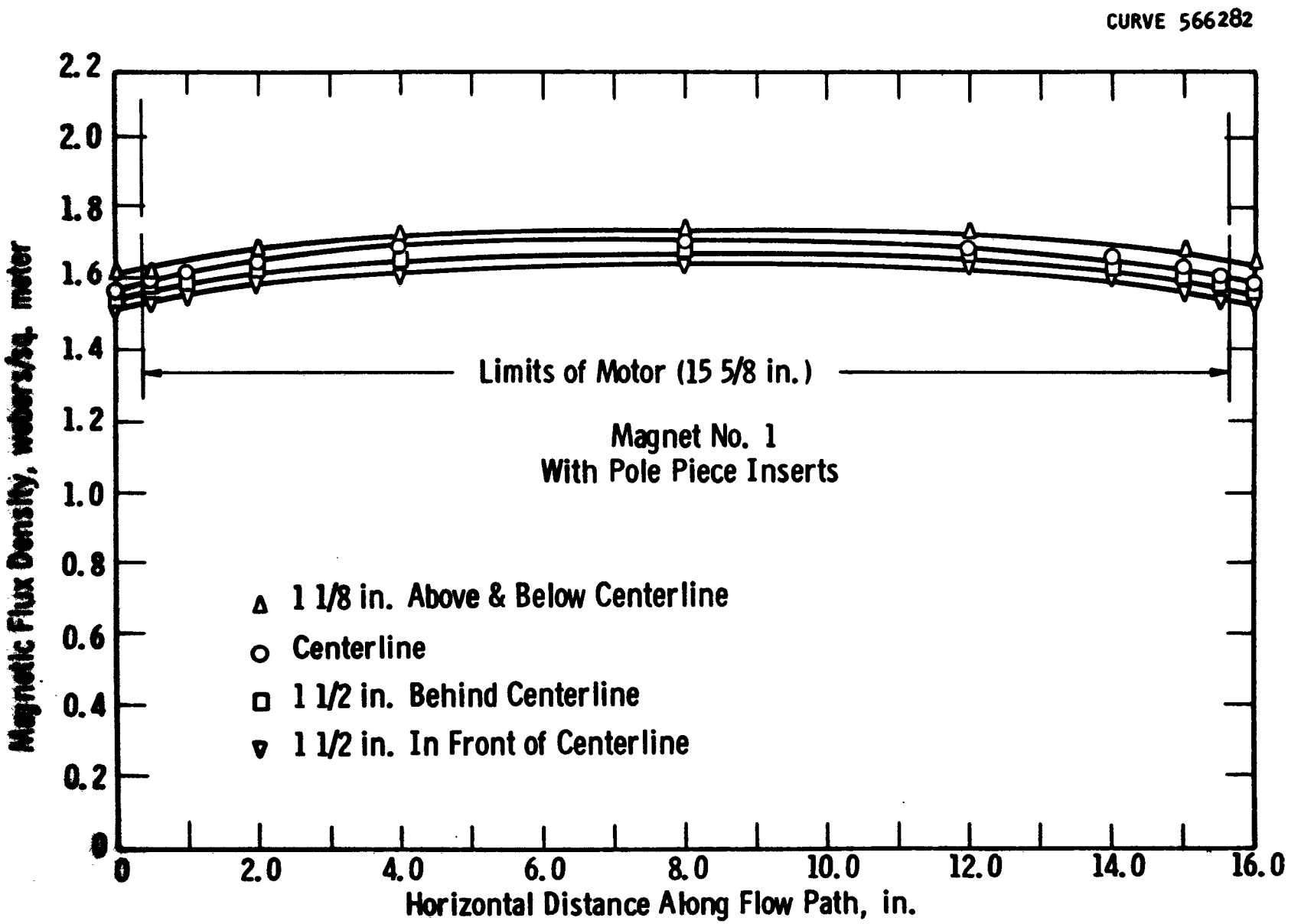

Fig. 17 - Magnetic Flux Mapping

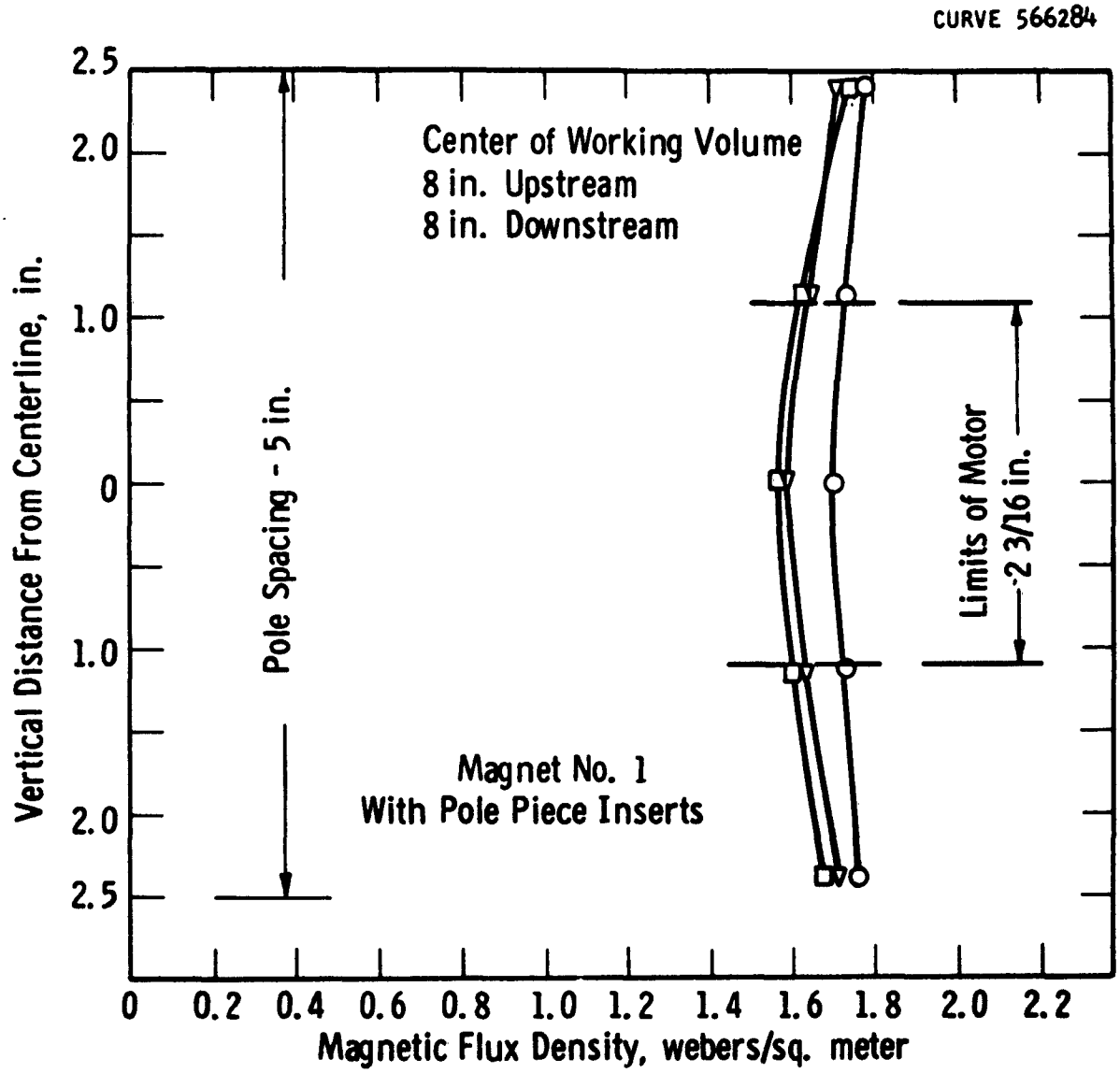

Fig. 18 - Magnetic Flux Mapping

CURVE 566283

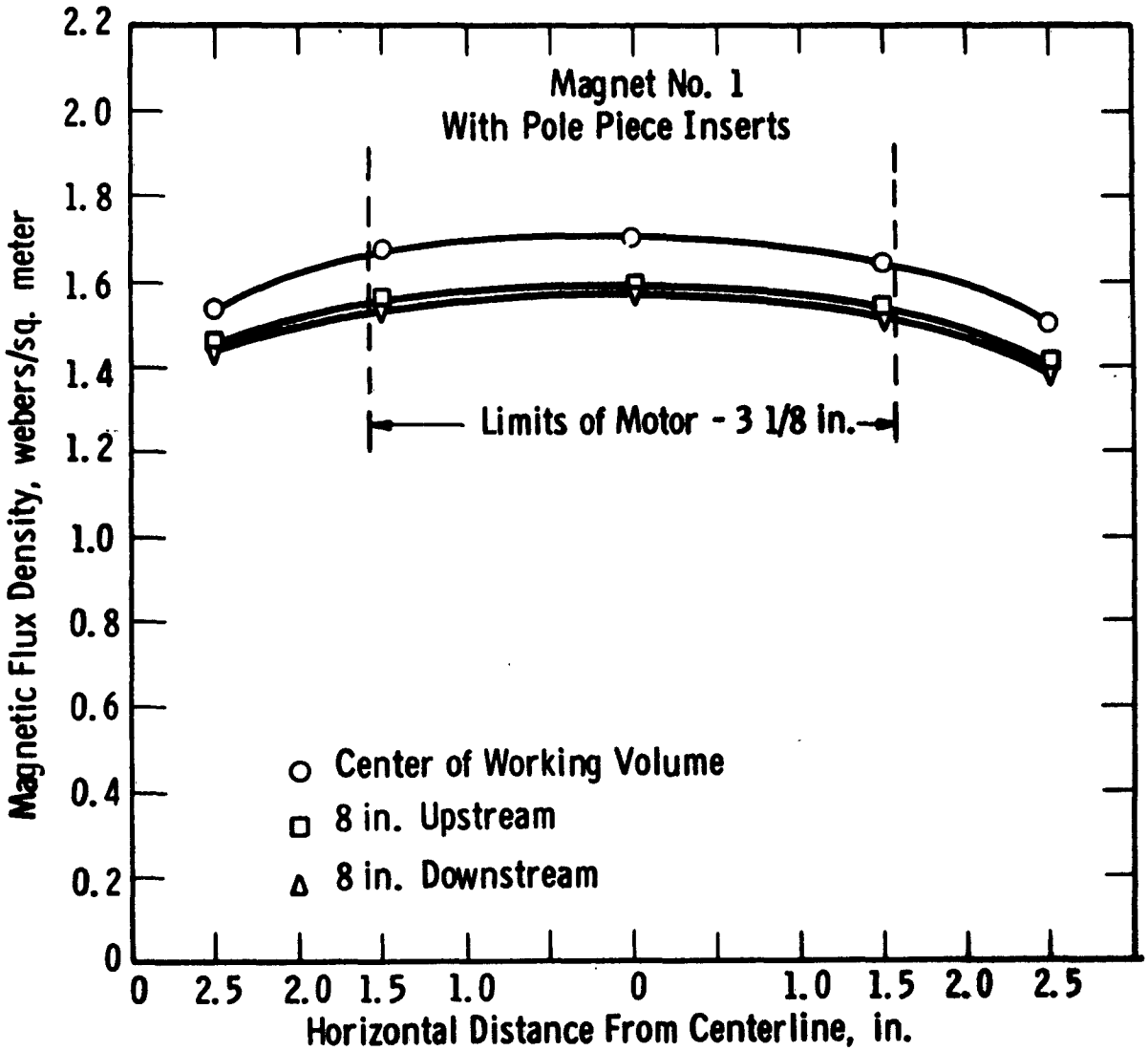

Fig. 19 - Magnetic Flux Mapping

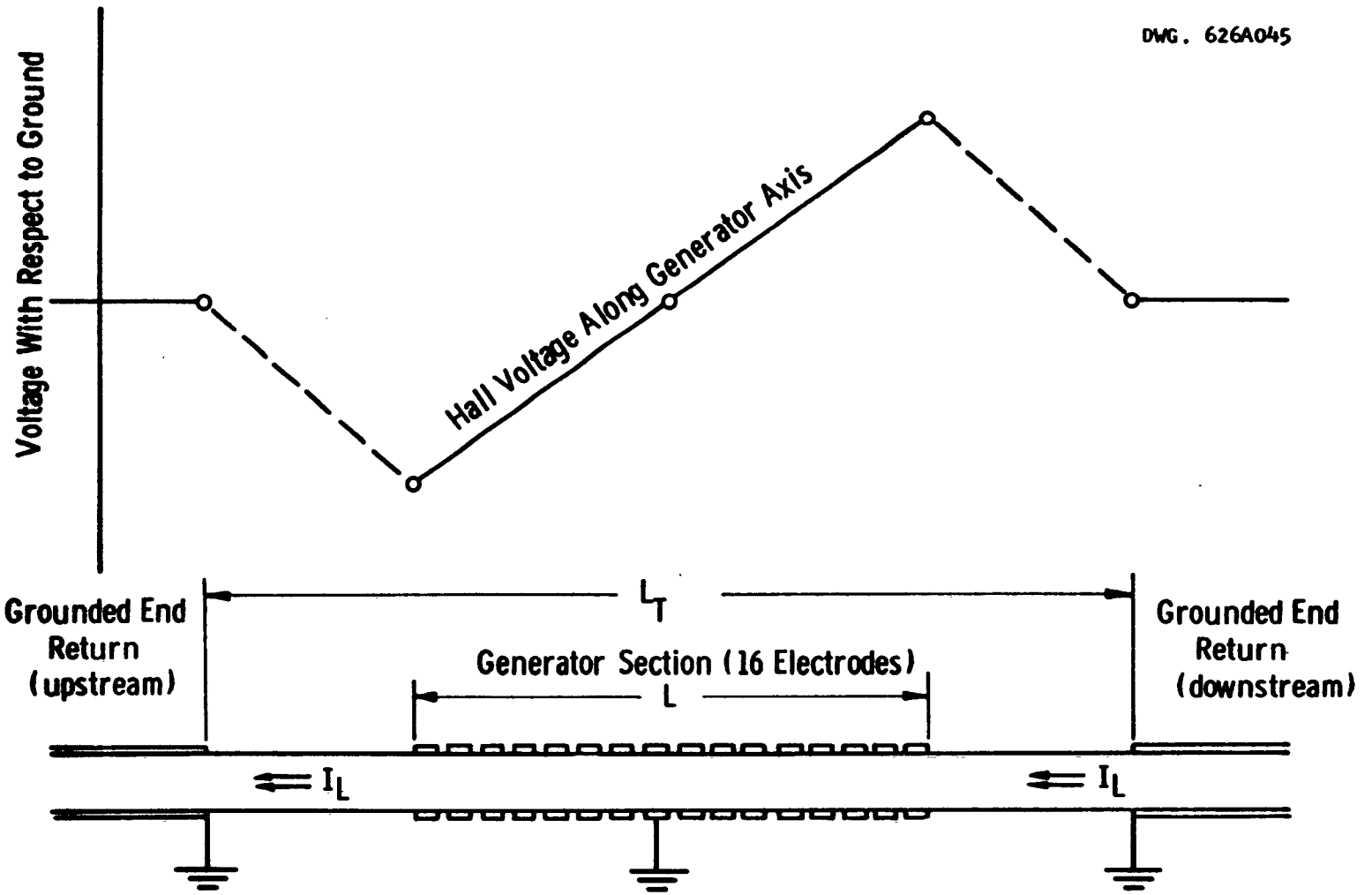

Fig. 20—Scheme illustrating end return power leakage

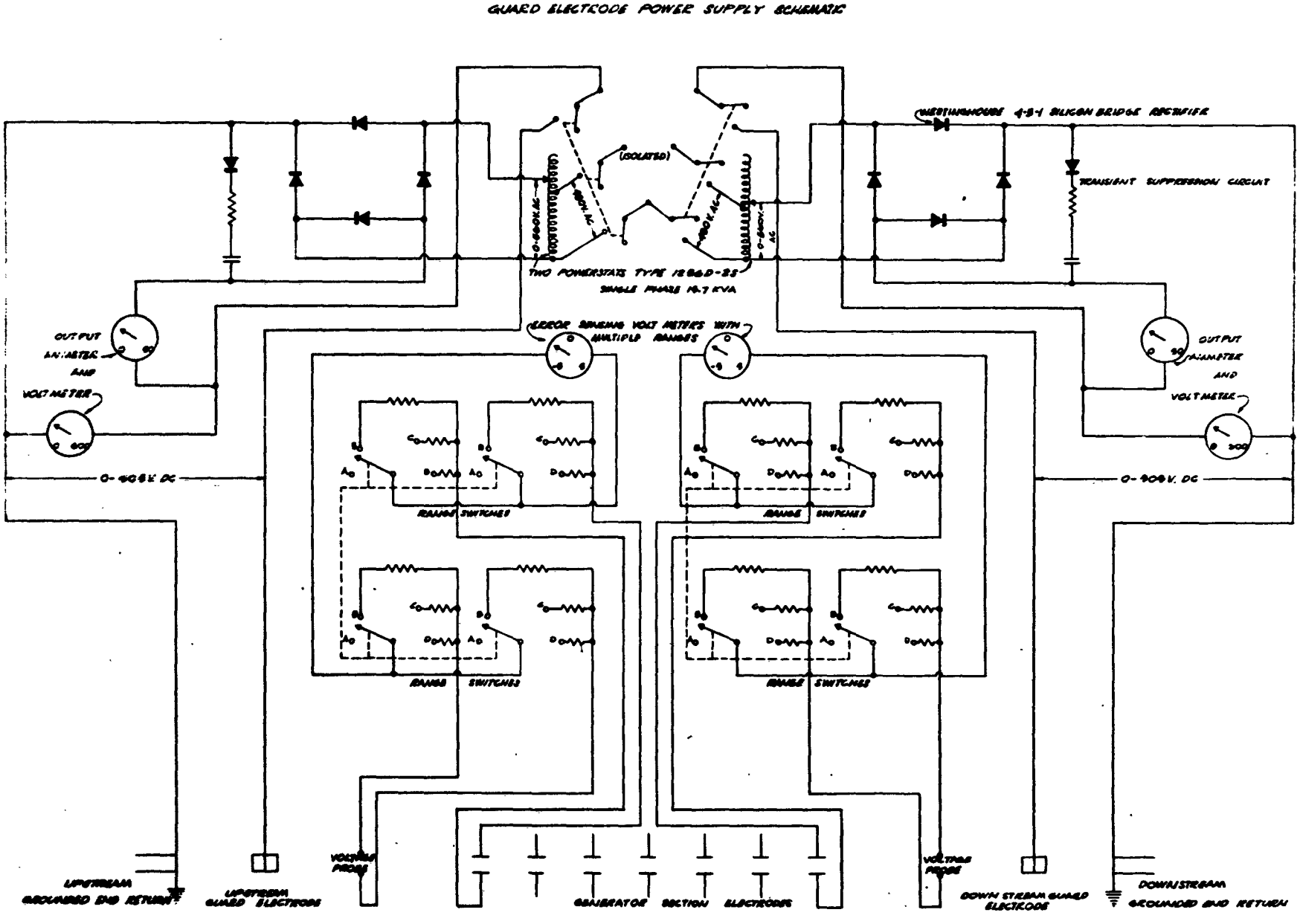

116C999

Fig. 21 - Guard Electrode Power Supply Schematic

Appendix B

GAS COOLED REACTORS FOR MAGNETOHYDRODYNAMIC POWER GENERATION

by

W. E. Gunson, E. E. Smith, J. H. Wright

Westinghouse Atomic Power Division
P. O. Box 355
Pittsburgh 30, Pennsylvania

T. C. Tsu

Westinghouse Research Laboratories
Beulah Road, Churchill Borough
Pittsburgh 35, Pennsylvania

GAS COOLED REACTORS FOR MHD POWER GENERATION

I. Introduction

The electric utility industry is one of the most progressive in the country, always looking for better, more efficient and more economic means of power generation. Since the turn of the century, there has been an eightfold increase in the electrical energy extracted for each unit of fuel used[1] with corresponding decrease in power cost. These improvements have been brought about by progressively better steam conditions, and today, modern generating plants are using super critical steam turbines at pressures of 5000 psi and temperatures in the range of 1100 - 1200°F.

In recent years, however, the rate of improvement in steam power plant performance has declined considerably, owing to the fact that steam plants now have much less room for improvement than previously. If further large gains in improvement are to be made, it seems that some new means of power generation must be developed. Among these new means that are somewhere over the horizon is the magnetohydrodynamic generator.

Reactor technology, of course, has been developing at a rapid pace over the past 15 years and considerable progress has been made toward the goal of economically competitive power generation by nuclear means. Historically, reactor temperatures have been relatively low,

the water reactors operating with coolant temperatures around 600°F and the highest to date being in the range of 900 to 1000°F. Experimental MHD generators on the other hand have utilized much higher temperatures, in the range of 4500 to 5000°F.

Recent activities in these two technologies, however, have shown some interesting trends. Reactor temperatures, while relatively low, have been moving steadily upward. They have gone, as mentioned previously, in recent years from 600 to nearly 1000°F, and reactors for much higher temperature operation are now being designed. With recent investigations in nonthermal ionization, the theoretical possibility now exists of generating power in an MHD duct at any temperature. The requirement for good cycle efficiency, however, imposes a lower limit on operating temperature.

The combination of these two developments is shown in Figure 1. The purpose of this paper is to outline the technical problems involved in combining a gas-cooled reactor with a MHD generator to form a closed loop power generation complex at a temperature which appears reasonably attractive for both concepts.

II.. Definition of Terms

Before discussing the design of a system and the problem areas involved, a brief treatment of some of the principles involved may be helpful. This section contains a very brief qualitative discussion of

MHD theory, brief mention of the types of equipment used in the power complex, and a discussion of the requirements for the working fluid.

A. Principles of MHD Power Generation

Magnetohydrodynamic (MHD) power generation is a method of direct energy conversion in which an electrically conducting gas moves through an enclosed duct in which a strong magnetic field is maintained, thereby converting part of the total enthalpy of the gas into electrical energy. Current is drawn off from electrodes along the sides of the duct. The process is similar to a conventional electrical generator, in which a solid conductor is moved through a magnetic field to obtain electricity. Other than the absence of moving parts in the MHD generator, the main difference is that in a gas, the "Hall effect" is much more pronounced than in a solid. Microscopically, this effect is the resultant of two types of electron motion: gyration around magnetic lines of force and collision with other atoms and molecules in the working gas. Macroscopically, this effect manifests itself in a displacement of the electric current vector. The magnitude of this effect is measured by the "Hall" coefficient $\omega\tau$, where ω is the electron cyclotron frequency and τ is the mean free time of electrons between collisions. In the design of an MHD generator, one has to consider not only the usual thermodynamic and hydrodynamic relations, but also the Hall effect and the electrodynamic relations given by Maxwell's equations.

The theory of MHD power generation has been considered by many investigators. In particular, the relation between Hall effect and generator configuration has been extensively treated.[2,3] Three generator configurations can be devised to give good performance characteristics for all values of $\omega\tau$: the continuous electrode configuration (Figure 2b) for $\omega\tau<1$, the Hall configuration (Figure 2c) for $\omega\tau>10$. The performance of the three generator configurations is summarized in Figure 3, where a non-dimensional power coefficient is plotted against generator efficiency for various values of $\omega\tau$.[3]

A good generator design should have reasonably high values of both efficiency and power density, the former for good overall thermal efficiency and the latter to keep the duct size from becoming excessive. Figure 3 shows that these conditions can be met by the continuous electrode generator for small values of $\omega\tau$, by the Hall type for large $\omega\tau$ and the segmented electrode for any $\omega\tau$. The segmented electrode type, however, has the disadvantage of being the most complicated of the three.

The theory of MHD generators has been firmly established. Many experimental units have been built and tested, in this country and abroad, ranging in size from a few watts to over one megawatt. Thus, the basic MHD principles are no longer in doubt, although many problem areas still remain.

B. Components Required for GCR-MHD Complex

The GCR-MHD system is a closed loop consisting of a reactor, a MHD duct and its auxiliary equipment including a cryogenic magnet, a steam generator-reheater and a compressor. A bottoming steam plant of conventional design improves overall cycle efficiency.

The high temperature reactor requires an unclad fuel design. Thus the system will have a high concentration of fission products, and provision for remote maintenance must be made. The core is approximately a right circular cylinder of graphite pierced by vertical fuel channels; the fuel elements are of the annular type. The reactor is designed to operate with an average outlet gas temperature of 3000°F.

The MHD generator is a rectangular duct designed for constant axial velocity. The required axial variation in duct cross section is achieved by expanding outward the top and bottom surfaces of the duct. The superconducting magnet coils for the MHD generator are positioned along the parallel vertical sides of the duct. Electrodes are located along the duct as shown schematically in Figure 2.

C. Coolant Requirements

Since the reactor coolant gas is also the MHD working fluid, its choice must be made from a combination of nuclear, heat transfer and thermodynamic considerations. For the HTGCR-MHD system discussed here, the best choice seems to be helium. Helium has negligible neutron

capture cross section, and it is stable to the action of radiation. It is chemically inert and has no harmful effects on structural or containment materials. Helium is not hazardous, which simplifies the problems of handling and storage. The low molecular weight and high specific heat of helium results in high heat transfer coefficient, relatively low reactor system pressure, and high gas velocities in the MHD duct. The use of helium also results in good electrical conductivity in the MHD generator, since electron mobility is quite high.

III. Cycle Description

An MHD generator can be used in a closed loop regenerative cycle for power production at reasonably good efficiencies. Considerably better efficiency, however, is obtained by using an MHD generator as a topping unit for a modern supercritical pressure steam plant. The reference design uses helium at 3000°F for the MHD generator. The bottoming unit uses steam at 3500 psi/1050°F with double reheat to 1050°F. The reference design cycle is shown in Figure 4.

Helium flows through the reactor at an average pressure of 104 psia and is heated to 3000°F. For the net power rating of 500 Mwe, a helium flow of 1,245,000 lb/hr is required.

The MHD unit supplies 315.5 Mwe, and an additional 400 MW is available from the steam cycle, which obtains its heat from the high temperature helium leaving the MHD unit. Helium leaves the MHD generator

at 2300°F and flows in series through the two steam reheaters and the steam generator. No extraction feedwater heating is used on the steam cycle, so that the helium temperature is reduced to a low value (275°F) in the steam generator to minimize compressor size. The helium compressor, which requies 168.4 MW, is driven by the steam turbine. Generator losses, DC-AC conversion equipment, cryogenic magnets, and other auxiliary loads require an additional 47.1 MW, leading a net output of 500 MWe. Reactor power requirement is 1062 MWt; overall plant efficiency is 47.1%.

IV. Design

A. Reactor

The design of the HTGCR was based on a thermal output of 1062 megawatts of heat. The average coolant outlet temperature was selected as 3000°F, as higher temperatures are probably feasible only for short-term operation, such as space application. For this outlet temperature, the fuel element is an unclad UC-graphite matrix. The maximum fuel center line temperature was limited to 4000°F by the fuel particle migration through the graphite matrix and the melting point of the fuel, UC, which is 4500°F. The coolant is helium for the reasons stated earlier.

A coolant inlet temperature of 648°F was selected based on the heat balance for the overall cycle. The coolant enters the reactor and flows downward between the inner and outer walls of the vessel,

cooling the outer wall before discharging into the plenum below the core, as shown in Figure 5. The coolant then flows upward through the core, removing the heat generated in the fuel, to obtain a 3000°F average outlet temperature. Fixed orifices located at the inlet distribute the flow 20% favorable to the hot channel. The hot gas then flows past an alkali metal seeding injector before entering the MHD generator.

The core design was optimized by a thermal analysis in which effects of fuel ring thickness to hydraulic diameter ratio, t/D_e, overall heat flux hot channel factor, F_q, core volume, and average heat flux, q''_{avg}, for a constant maximum fuel center line temperature of 4000°F were studied. The result is shown in Figure 6. It is mandatory when determining the values of heat flux, t/D_e, core volume, and F_q, that a "square" be completed as illustrated for this design. From the initially selected fuel ring thickness, t, and t/D_e, a line is drawn horizontally through q''_{avg} to the selected F_q and then drawn vertically down to the t/D_e curve in the third quadrant, horizontally to the diagonal base line and then vertically to the t/D_e curve in the first quadrant. The t/D_e in the third quadrant must match with the pre-selected t/D_e ratio in the first quadrant (a miss-match indicates either higher or lower fuel center temperature). A more detailed treatment of this method, for a somewhat different design, is given in Reference 4.

The fuel element consists of two concentric annular rings around a center rod. The thickness of the fuel ring is 0.375 in.

The diameter of the center rod is twice the fuel ring thickness. The fuel is UC dispersed in a graphite matrix. A cross section of the fuel element, with dimensions, is shown in Figure 7.

The active core approximates a right circular cylinder 23.2 ft. in diameter and 23.2 ft. in height. The number of fuel channels is 602, pitched in a square array on 10 inch centers. The reflector regions, radial, top and bottom, are two and one-half feet thick. The moderator and reflectors are AGOT grade graphite.

The total heat transfer area is 51,000 ft^2, giving an average heat flux of 71,000 Btu/hr. ft^2. The maximum heat flux, which exists in the hot channel is 163,000 Btu/hr. ft^2. The maximum fuel center line temperature is 3922°F. A summary of the core and reactor performance data is given in Table 1.

The use of a high temperature unclad ceramic fuel results in the diffusion of a relatively high percentage of fission products into the coolant stream. These relatively high activity levels necessitate provision for remote maintenance of plant components. Piping, thermal insulation and other vulnerable components are designed to be remotely replaceable.

Table 1

500 MWe GCR-MHD Design Data

Reactor:	
Thermal Output, MW(t)	1062
Coolant Inlet Temperature, °F	648
Coolant Outlet Temperature, °F	3000
Coolant Flow, lb/hr	1.245×10^6
Core:	
Equivalent Diameter, ft	23.2
Core Height, ft	23.2
Average Heat Flux, Btu/hr-ft^2	71,000
Maximum Heat Flux, Btu/hr-ft^2	163,000
Total Heat Transfer Area, ft^2	51,000
Total Flow Area, ft^2	51.0
Active Core Volume, ft^3	9,700
Maximum Fuel Center Line Temp., °F	3922
Average Coolant Velocity, ft/sec	400
Power Density, kw/liter	3.9

B. MHD Generator

For reasons discussed below, the MHD generator used in this design is of the segmented electrode configuration. The principle dimensions and characteristics of the MHD generator are shown in Figure 8. The segmented-electrode configuration requires the use of many pairs of electrodes, perhaps as many as 100 pairs. For this reason, it is not so desirable as the Hall configuration, but for this particular design, the segmented electrode was the only workable solution.

The generator length of 90' may appear greater than might be desired. This disadvantage, however, could be removed by doubling up the generator into a U-shaped duct, and using an elbow to reverse the flow. Some flow loss would be incurred, but the generator length could be cut approximately in half.

The generator electrodes may be made of graphite, tungsten, molybdenum, or zirconium. A suitable insulating material for the top and bottom walls and the spacers between electrodes may be zirconia, alumina, magnesia, or some other refractory oxide.

The superconducting magnet, shown schematically in Figure 9, consists of many layers of coils wound from niobium-tin and niobium-zirconium wires, maintained at liquid helium temperature. Extensive investigations have shown that thermal insulation between the hot gas inside the MHD duct and the liquid helium required for superconducting should present no serious problem. The power required to operate the cryogenic system is a very small fraction (less than one per cent) of the MHD output.

In designing the MHD generator, it was assumed that a magnetic flux density, B, of 10 weber/m^2 is obtainable from the superconducting magnet. While this is somewhat beyond present technology, it is within the realm of possibility for future operation. The mean static temperature in the MHD generator is 1424°K (2561°R) and the mean static pressure is 3.2×10^5 Newton/m^2 (46.4 psia). Hence, the gas density N is 1.628×10^{25} particles/m^3 (MKS units are used for convenience throughout this

analysis). The electron mobility is given in Figure 10.[5] This shows that at 1424°K, $\mu N = 1.14 \times 10^{25}$ m^{-1} $volt^{-1}$ sec^{-1}, and hence the electron mobility, μ, is 0.70 $m^2/(volt)(sec)$. Thus $\omega\tau = \mu B = 7$. Since this value is between 1 and 10, a segmented electrode generator configuration is selected. To obtain a generator efficiency of 80%, the loading parameter[3]

$$q = \frac{\text{load resistance}}{\text{load resistance + internal resistance}} = \frac{E_y}{ub} = 0.8 \qquad (1)$$

where E_y is the external electric field in the y - direction (refer to Figure 2a).

To operate the generator at 1424°K, some form of non-thermal ionization is necessary. The possible methods include electron heating ionization (Kerrebrock effect), electron injection, and fission product ionization. Previous work[6] has indicated that the magnitude of ionization attainable by fission products is insufficient. Of the other two methods, the Kerrebrock effect is preferable because of the arrangement complexity of the electron injection equipment. Ionization phenomena are discussed in detail in Section V, and the problems involved in achieving the necessary ionization are outlined in Section VI.

Ionization by the Kerrebrock effect involves seeding the working fluid with alkali metal. The concentration required is such that a large part of the metal condenses in the low temperature portions of the cycle.

A system for collecting and re-injecting the condensate is, therefore, required.

Using the ionization parameters calculated in Section V and the constants already given, the current density, j_y, is calculated to be 934 amps/m^2. The pressure gradient along the generator is

$$\frac{dp}{dx} = j_y B \quad .$$

This equation defines the required duct length, which is 27.5 m or 90'.

C. Other Components

Besides the nuclear reactor and the MHD generator, other major components of the system complex are the helium compressor, the steam superheater, reheater, and evaporator heat exchangers, the D.C. to A.C. inverters, the alkali metal injection seeding equipment, and the connecting piping.

The helium compressor is of the multi-stage, axial flow type design for a minimum of maintenance. As the gas contains fission products, all maintenance must be done remotely. Depending on the level of activity and the characteristics of the compressor, it can be shaft driven off the steam turbine-generator unit or by a separate steam turbine drive unit. The pressure ratio across the compressor is 2.34:1 and the inlet temperature is 275°F. At this inlet temperature, a large part of the alkali metal seeding required, according to present

estimates of the Kerrebrock effect, will condense before passing through the compressor. A system for recovery and re-injection is, therefore, required.

The compound heat exchanger, consisting of superheater, reheater and evaporator, for the steam bottoming cycle is of conventional design. The high temperature differential between the helium gas and the steam in the superheater and reheater imposes design limitations concerning thermal stresses, thermal shock, and thermal expansion. The tube and shell materials are a high temperature-high strength alloy.

The D.C. to A.C. inverters utilize ignitron vacuum tubes which are of conventional design. Inverters using solid state devices may become available by the time required by the MHD application.

The connecting piping between the reactor vessel and the MHD duct and between the MHD duct and the heat exchanger is internally insulated so that the pipe wall temperature will not exceed 900°F. The internal insulation is comprised of multi-layers of ZrO_2, SiO_2 and stainless steel baffles.

V. Methods of Non-Thermal Ionization

As pointed out earlier, several alternative methods of non-thermal ionization are available and have been analyzed in some detail. Of the methods available, ionization by electron heating is the most

attractive possibility. If this should not be feasible, electron injection is available as an alternate, although this involves some rather complex problems in equipment arrangement and reliability.

Since an unclad fuel is used, the coolant necessarily contains a high concentration of fission products. The activity from these products provides some ionization, but the necessary ionization probably cannot be achieved by fission products alone.[6] Therefore, no further discussion of this aspect will be made.

Although the preferred method of ionization is by the Kerrebrock effect, the calculations are such that it is simpler to analyze the electron injection case first and then match the requirements for the Kerrebrock effect to it. This is the method used below.

A. Electron Injection

In this method, electrons are introduced from an external source and collide with the helium atoms to ionize them. The power required for ionizing a unit volume of gas is given by[6]

$$P_i^* = \alpha n^2 \phi \times 1.6 \times 10^{-19} \qquad (2)$$

The power density of a segmented-electrode generator is[2,3]

$$P_g^* = \sigma u^2 B^2 q (1-q) \qquad (3)$$

If the power consumption by the electron generators is limited to 2% of the generated MHD power, then

$$\frac{P_i^*}{P_g^*} = 0.02 = \frac{\alpha n^2 \phi \times 1.6 \times 10^{-19}}{\sigma' u^2 B^2 q (1-q)} \qquad (4)$$

But $\sigma' = ne\mu$ (5)

where e is the electronic charge. Combining (4) and (5) results in

$$\frac{\alpha n \phi \times 1.6 \times 10^{-19}}{e \mu u^2 B^2 q (1-q)} = 0.02 \qquad (6)$$

A reasonable value for α in pure helium is 10^{-14} $m^3/sec.$[7] Upon substitution of the appropriate values into (6) the electron density, n, is found to be 2.35×10^{18} electrons/m^3. It then follows that $\sigma' = 0.263$ mho/m, $P_g^* = 1.326 \times 10^7$ watts/m^3. The required generator volume is $3.155 \times 10^8 / 1.326 \times 10^7 = 23.8$ m^3. The current-voltage characteristics can now be easily calculated by using the appropriate formulas in reference 2 or 3. The results are $E_x = 24{,}850$ volts/m, $E_y = 14{,}200$ volts/m, $j_y = 934$ amp/m^2. The current density j_y is rather modest and should not cause any electrode problem. The pressure gradient along the length of the generator is

$$\frac{dp}{dx} = j_y B = 9340 \text{ Newt/m}^3 \quad .$$

Since the pressure drop across the generator is 2.567×10^5 Newt/m^2 (37.23 psi), the required generator length is

$$L_g = \frac{2.567 \times 10^5}{9340} = 27.5 \text{ m (90 ft)}$$

The voltage output is E_y x (distance between electrodes) = 14,200 x 0.813 = 11,550 volts.

One pertinent question may be asked. How many electron generators are required? In other words, what is the distance between adjacent guns? Since the injected electrons recombine with positive ions, they need to be constantly replenished. The rate at which electrons are lost by recombination is given by

$$\frac{dn}{dt} = - \alpha n^2 \qquad (7)$$

Thus the time it takes for any electron density, n, to decrease to half its original value, n/2, is

$$\tau = \int_0^{\tau} dt = - \frac{1}{\alpha} \int_n^{n/2} \frac{dn}{n^2} = \frac{1}{\alpha n} \qquad (8)$$

By substituion, the time is found to be 4.26×10^{-5} sec. Since the gas is moving at a velocity of 1775 m/sec, the distance between adjacent generators should be $\Delta u = (4.26 \times 10^{-5})(1775) = 0.0756$ m (3 inches). This is the required distance if the electron density is allowed to fluctuate between 2.35×10^{18} and 1.18×10^{18} m^{-3}, which is not an unreasonable assumption.

Based on this spacing, then, a total of about 360 generators is needed along the entire length of the generator. This is one of the principal objections to this method of ionization. The complication arising from the use of this many electron generators may necessitate excessive maintenance. In the calculations, a recombination coefficient for pure helium was used. The inclusion of impurities in the reactor coolant gas adversely affects the results. Even if a purification system is used, the presence of some impurities is unavoidable. Additional information regarding the effect of impurities on recombination appears necessary.

B. Electron Heating Ionization

This method is based on the well known phenomenon that in most low-pressure discharges the ionization results from electron impact and that the average electron energy is many times the thermal value. The same phenomenon is seen in the Townsend drift tube. The reason is that the energy gained by the electrons moving in the electric field is only inefficiently transferred to the heavy molecules through elastic

collisions. The application of this phenomenon to enhance ionization in an MHD generator was first proposed by Professor Kerrebrock.(8) Hence this method has become known as the "Kerrebrock effect".

Under the influence of this effect, the electron temperature (T_e) in an MHD generator can be considerably higher than the total temperature (T_t) of the gas. The relation between these temperatures in a segmented-electrode generator is given by(9)

$$\frac{T_e}{T_t} = \frac{1 + \frac{1}{3}\gamma\beta^2 M^2 \delta^{-1} (1-q)^2}{1 + \frac{1}{2}(\gamma - 1) M^2} \qquad (9)$$

In using equation (9), the precaution should be taken that μ (used in computing $\beta = \mu B$) is a function of T_e as indicated in Figure 10. They should be consistent. Thus a trial and error solution is in general necessary. Such a procedure was followed and the results below were obtained:

T_{e_1} = 2155°K (at inlet of generator)
T_{e_2} = 1766°K (at exit of generator)
T_e = 1960°K (mean value)
μ = 0.515 m^2/(volt)(sec)
$\beta = \mu B = 5.15$

The helium gas is seeded with cesium vapor which has a very low ionization potential. The degree to which cesium is ionized may be calculated

from Saha's equation:

$$\frac{f^2}{1 - f^2} = 0.0335 \frac{T_e^{5/2}}{p_{cs}} \exp\left(-\frac{e V_i}{k T_e}\right) \qquad (10)$$

But $P_{cs} = \epsilon p$.

Substituting the appropriate constants gives

$$\frac{\epsilon f^2}{1 - f^2} = 2.04 \times 10^{-9} \qquad (11)$$

The electrical conductivity σ' is given by:

$$\sigma' = ne \mu = (N \epsilon f) e \mu \qquad (12)$$

The same conductivity as that in the electron injection case (0.263 mho/m) is used. Since $N = 1.628 \times 10^{25}$ m^{-3},

$$\epsilon f = 1.96 \times 10^{-7} \qquad (13)$$

A simultaneous solution of equations (11) and (13) gives $\epsilon = 1.88 \times 10^{-5}$ and $f = 0.0104$. Thus the seeding ratio is about 2 atoms of cesium for each 10^5 atoms of He. About 1% of the cesium is ionized.

Under the above conditions, the characteristics of the MHD generator are the same as those in the electron injection case. Thus the dimensions, power output, voltage output, current density, and efficiency are all the same. The only difference is in E_x (voltage gradient along length of generator), since here $\mu B = 5.15$ whereas formerly it was 7.

The lowest temperature of the cycle (Figure 4) occurs at the compressor inlet. At this point the partial pressure of cesium is 5.86×10^{-5} atm. The corresponding dew point is 382°F. Since the actual gas temperature is 275°F, some of the cesium vapor will condense into liquid; the amount is estimated to be 93%. This condensate should be removed and reinjected at the MHD generator inlet.

VI. Problem Areas

The problems inherent in the GCR-MHD concept fall into two categories: systems problems, or those problems resulting directly from the combination of a high temperature gas cooled reactor, and a MHD generator in a closed loop and component problems resulting for the most part from high temperature service required. The investigations reported in this paper have pointed out many of the areas which require resolution, but the problems have by no means been solved. Many points require further analysis and experimental verification.

A. Systems Problems

One of the main systems problems is that of the proper operating pressure. Reactor design considerations, such as heat transfer coefficient, fuel inventory, core size, etc. require high gas pressure, while low pressure is preferable for operation of the MHD generator. The reactor heat transfer coefficient, for equal gas velocities through the core, is proportional to the eight-tenths power of the system pressure. The core volume, assuming constant unit fuel cell design, varies as the 1.25 power of the pressure level. The fuel loading varies approximately linearly with the core volume.

As far as the MHD generator is concerned, the operating pressure should be low. First of all, the electron mobility is inversely proportional to pressure. Low pressure leads to high electron mobility and high $\omega\tau$. Secondly, at a given temperature and a given seeding ratio, gas conductivity varies inversely as the square root of gas pressure.[11] Thirdly, reducing the pressure would result in a more favorable generator geometry.

The choice of pressure and other parameters for the design resulted in the necessity for a segmented electrode generator configuration. If at all possible, the Hall configuration would be preferable. Perhaps a somewhat lower generator efficiency, a somewhat lower pressure or a combination of both could be accepted to gain the advantage of the better generator configuration. This point requires considerable further investigation.

It is not known whether either method of non-thermal ionization discussed above is feasible. While electrons are known to cause ionization, the uncertainty of electron injection lies in the mechanism and extent of recombination. Small amounts of impurities, particularly those with strong electron affinity such as iodine and bromine, may render this method unworkable with high concentrations of fission products. To establish the maximum permissible limits of impurities, it appears that recombination measurements in an actual or simulated reactor coolant gas will be needed. The other objection, mentioned once before, is the complexity and maintenance problem involved in the use of many electron generators.

The uncertainty of the electron heating method is more fundamental. While both Kerrebrock[8] and Robben[10] have observed substantial conductivity enhancement in the absence of a magnetic field, the latter found no evidence of non-equilibrium ionization when a magnetic field was applied. This point is being given further intensive investigation in several laboratories. If the basic theory could be confirmed experimentally, its application to actual MHD generators would be very simple and most attractive.

Small amounts of impurities may have very important effects on the MHD process, some of which have already been mentioned. Firstly, they greatly increase the electron loss rate, especially the halogens such as iodine and bromine. Secondly, they decrease the electron mobility.[14] Thirdly, they greatly increase the energy loss parameter δ of equation (9). While this parameter is approximately unity for

monatomic gases, it could be 100, 1000, or larger for diatomic and polyatomic molecules. From equation (9), it may be seen that a large value of δ can easily nullify the electron heating or Kerrebrock effect.

All things considered, it appears that an efficient helium purification system will be necessary. Additional experimental information will be needed to establish the tolerable impurity levels, however.

In the electron heating method of ionization, cesium was used as the seeding material because of its low ionization potential. Even so, the concentration required is such that a large fraction condenses in low temperature portions of the cycle. It may be more attractive to maintain the cesium vaporized by raising the low temperature, thereby suffering some penalty in efficiency but eliminating the necessity for a cesium recovery and reinjection system.

Cesium is quite expensive, and any material lost by deposition must be made up at an economic burden to the system. In addition, cesium is quite corrosive, and that portion which remains vaporized and is carried through the core may react with the reactor materials. Any cesium remaining in the core would add to the economic burden and would also result in a severe penalty from the standpoint of neutron economy.

Its neutron capture cross-section is larger than could be desired. It is expensive. If cesium proves to be unacceptable, two other possible seeding materials are UO_2 and Ba_2O. The former has an ionization potential of 4.3 volts[12] and the latter, 4.0 volts.[13]

These are about comparable to potassium. However, both UO_2 and Ba_2O have very low vapor pressures.[12,13] If they were to be used, special provisions would have to be made to generate and maintain the necessary concentrations in the MHD duct.

The effects of high magnetic and electric field intensity and of current density on the various parameters requires further investigation. The effects of shape and current density on electrode current leakage and possible sparking is one of the many other problem areas requiring further investigation.

B. Component Problems

In addition to the already mentioned problems and study areas associated with the overall HTGCR-MHD system, several critical areas, where positive information is lacking, must be investigated. These areas are associated with materials, insulation, and maintenance.

The high temperatures and the high gas velocities encountered in the HTGCR-MHD complex impose a number of materials problems. The core will be built up by stacking blocks of graphite which are pierced by the fuel channels. Thus the stability and the thermal properties of the graphite need to be established in the presence of radiation at 3000°F.

The fuel element design must be proven as the maximum temperature limit is set by the melting temperature of the fuel particles, the limit of stability for the fuel particle or the matrix material, the

rate of fuel particle migration through the fuel element matrix and the rate of diffusion of fission products through the matrix material. The high gas velocity, 400 fps and higher, through the core requires the fuel element and the graphite moderator to have good corrosion and erosion properties.

The outlet gas temperature of 3000°F requires the reactor vessel to be of double wall construction with high temperature insulation internally on the inner wall in order to keep the outer wall temperature below 1000°F. Both walls, inner and outer, require a high temperature ferritic material.

The internal insulation used in the piping and the MHD generator must remain intact for an extended period of time at 3000°F. The corrosion and erosion resistance of the insulation and the electrodes used in the MHD generator must be evaluated at 3000°F in the presence of gas velocities approaching 2000 meters per sec. to establish the lifetime for replacement. Very high magnetic fields are required for this concept - even beyond the realm of present experimental technology with superconducting magnets. The feasibility of these magnets for long term service must be established.

The HTGCR-MHD system is a dirty system as the fission products diffusing out of the unclad fuel elements are carried throughout the primary system by the helium. All parts of the primary systems, must be designed for minimum routine maintenance as all maintenance and repair must be done remotely. The helium compressor must be designed for decontamination and must be capable of remote removal and replacement

by cutting and welding at predetermined points. The auxiliary equipment requiring regular maintenance must be located in a hot cell arrangement equipped with manipulators and special tools.

VII. Conclusions

This paper has attempted to show one attractive possibility for future power generation. However, as has been demonstrated, the concept of the GCR-MHD complex involves manifold problems. Not enough is known at present even to guess at the possible economics of this concept. Indeed much more investigation must be undertaken before even the technical feasibility can be considered certain, and a great deal of experimental work remains to be done in the years to come. The concept does offer a very attractive possibility for high efficiency power generation if the many problems outlined in this paper can be solved.

VIII. Acknowledgements

The authors extend grateful thanks to L. S. Frost and W. A. Stewart of the Westinghouse Research Laboratories for their helpful discussions of electron mobility and superconducting magnets.

Nomenclature

A	Area, ft^2 or m^2
B	Magnetic flux density, webers/m^2
D_e	Hydraulic diameter, ft
e	Electron charge, 1.6×10^{-19} Coulomb
E	Electric field, volts/m
f	Ionization fraction, ratio of ionized seed to total seed
F_q	Heat flux hot channel factor
j	Current density, amps/m^2
k	Boltzmann's constant, 1.38×10^{-23} joule/°K
L	Length, ft or m
M	Mach number
n	Electron or ion density, m^{-3}
N	Particle density, m^{-3}
P	Static pressure, psi or newtons/m^2
P_{cs}	Partial pressure of cesium
P_t	Total pressure
P^*	Power density, w/m^3
q	Generator loading parameter, ratio of external to total resistance
q"	Heat flux, Btu/hr ft^2-°F
t	Fuel thickness, ft
T	Static temperature, °K or °R
T_e	Electron temperature
T_t	Total temperature

Nomenclature (cont'd)

u	Velocity, ft/sec or m/sec
V_i	Ionization potential, ev
α	Recombination coefficient, m^3/sec
β	Hall coefficient ($\omega\tau$)
γ	Ratio of specific heats (5/3 for helium)
δ	Energy loss parameter (unity for monatomic gases)
ζ	Electron half-life, sec.
μ	Electron mobility, m^2/volt sec.
σ	Electrical conductivity of gas, mho/m
τ	Electron mean free time between collisions, sec.
ϕ	Energy of formation of ion pairs, ev
ω	Electron cyclotron frequency, sec^{-1}
ϵ	Seeding ratio, atomic fraction of seed material
η	Efficiency

References

1) P. Spron, Statement to the Joint Committee on Atomic Energy, 202 Hearings; May 1962.

2) S. Way, "Remarks on High Magnetic Fields in MHD Generators," Westinghouse Research Memo 311-H000-M2; March 1, 1961.

3) L. P. Harris and J. D. Cobine, "The Significance of the Hall Effect for Three MHD Generator Configurations," Trans. ASME (J. Engineering for Power), Vol. 83(1), Series A, pp. 392-396; October 1961.

4) F. S. Bloxam, W. E. Gunson, and I. M. Keyfitz, "High Temperature Gas Cooled Reactor Magnetohydrodynamic Power Unit Study," Westinghouse Atomic Power Division Report WCAP-1884; November 1961.

5) L. S. Frost, Westinghouse Research Laboratories, Private Communication, 1962.

6) E. J. Sternglass, T. C. Tsu, G. L. Griffith, and J. H. Wright, "MHD Power Generation by Non-Thermal Ionization and Its Application to Nuclear Energy Conversion," Paper presented at the Third Symposium on Engineering Aspects of MHD, Rochester, New York; March 28-30, 1962.

7) C. L. Chen, C. C. Leiby, and L. Goldstein, "Electron Temperature Dependence of the Recombination Coefficient in Pure Helium," Phys. Rev., Vol. 121, pp. 1391-1400; March 1961.

8) J. L. Kerrebrock, "Conduction in Gases with Elevated Electron Temperature," Paper presented at the Second Symposium on Engineering Aspects of MHD, Philadelphia, Pa.; March 9-10, 1961.

9) H. Hurwitz, Jr., G. W. Sutton, and S. Tamor, "Electron Heating in Magnetohydrodynamic Power Generators," ARS Jour., Vol. 32, pp. 1237-1243; August 1962.

10) F. Robben, "Non-Equilibrium Ionization in a Magnetohydrodynamic Generator," Phys. Fluids, Vol. 5, pp. 1308-9; October 1962.

11) S. Way, S. M. DeCorso, R. L. Humdstad, G. A. Kemeny, W. A. Stewart, and W. E. Young, "Experiments with MHD Power Generation," Trans. ASME (J. Engineering for Power), Vol. 83(1), Series A, pp. 397-408; October 1961.

12) G. DeMaria, R. P. Burns, J. Drowart, and M. G. Inghram, "Mass Spectrometric Study of Gaseous Molybdenum, Tungsten, and Uranium Oxides," J. Chem. Phys.; Vol. 32, pp. 1373-1377, May 1960.

References (cont'd)

13) M. G. Inghram, W. A. Chupka, and R. F. Porter, "Mass Spectrometric Study of Barium Oxide Vapor," J. Chem. Phys. Vol. 23, pp. 2159-2165; November 1955.

14) L. S. Frost, "Conductivity of Seeded Atmospheric Pressure Plasmas," J. Appl. Phys., Vol. 32, pp. 2029-2036; October 1961.

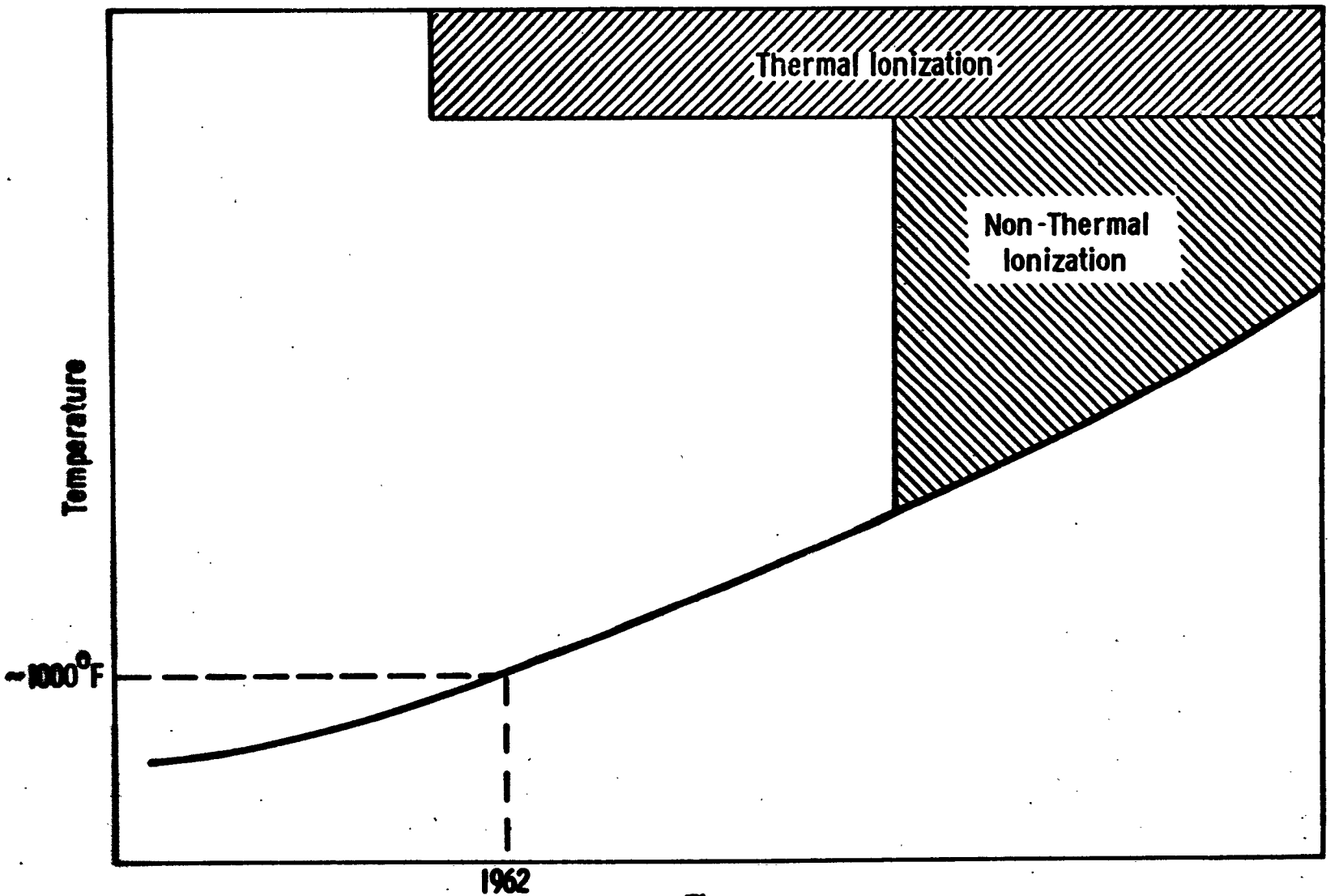

TRENDS IN REACTOR AND MHD TECHNOLOGY E. D. SK 297631 B

Fig. 1

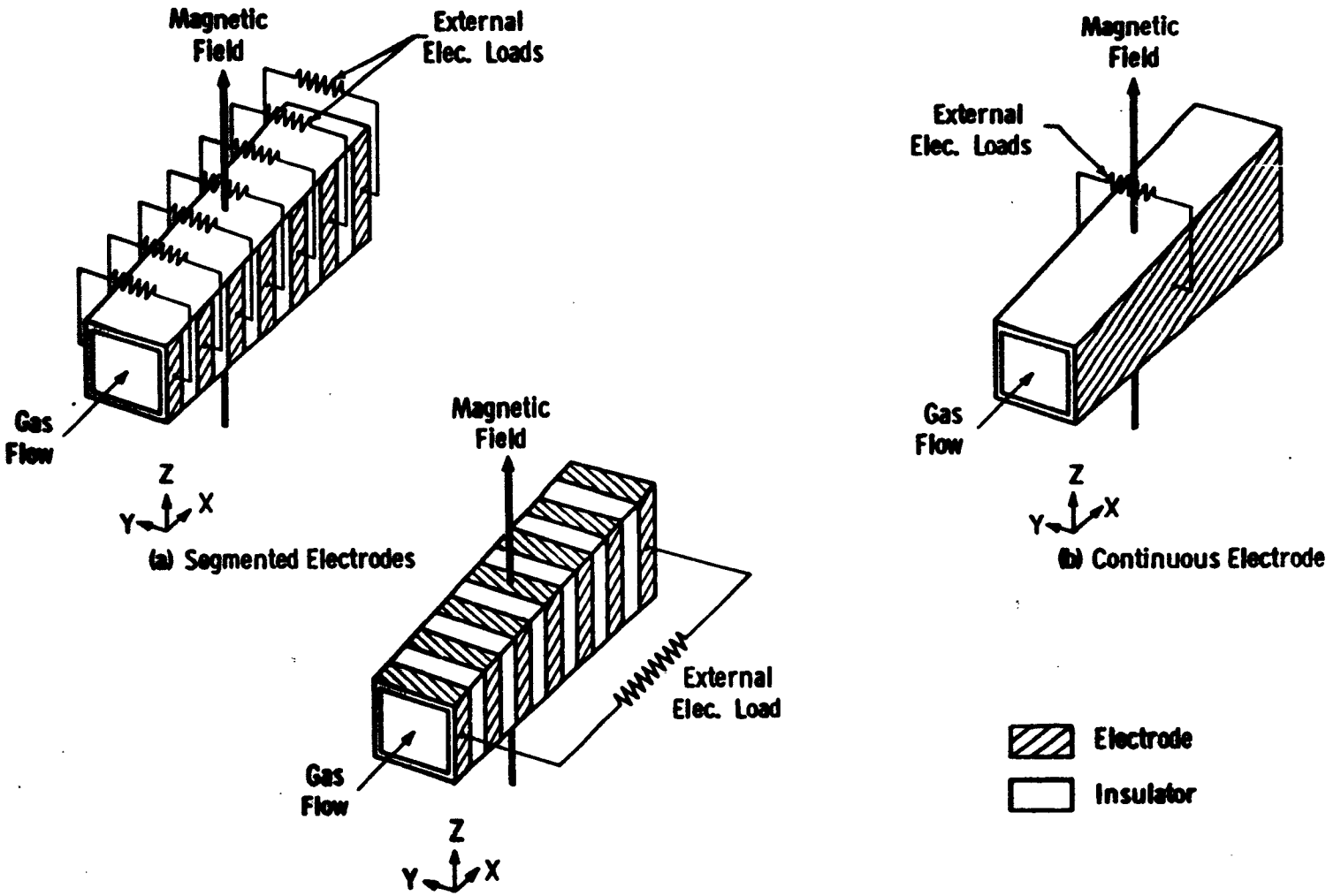

SCHEMATIC REPRESENTATION OF MHD GENERATORS

Fig. 2

E. D. SK 297630 B

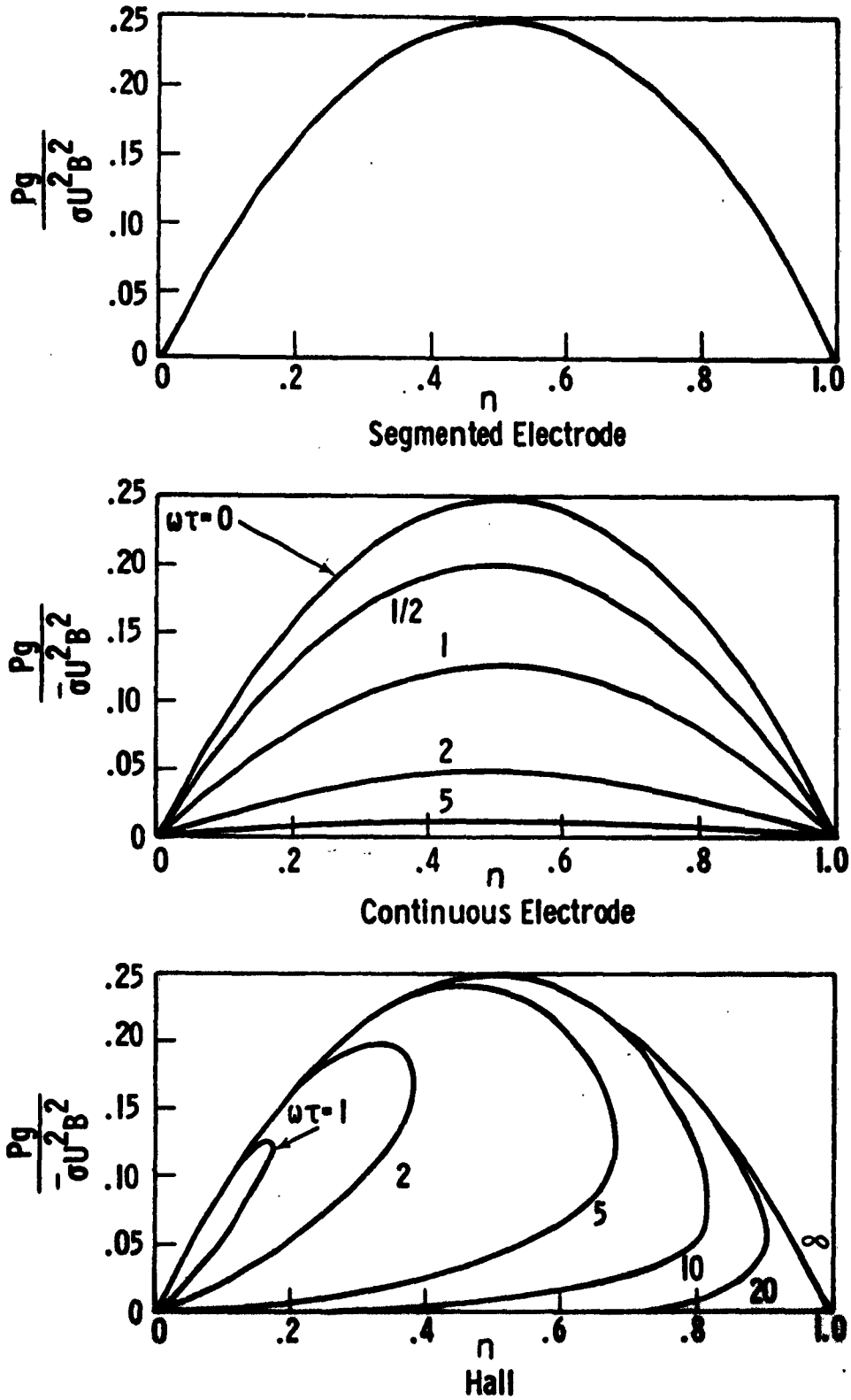

RELATIONS BETWEEN POWER & EFFICIENCY

Fig. 3

E. D. SK. 297634 B

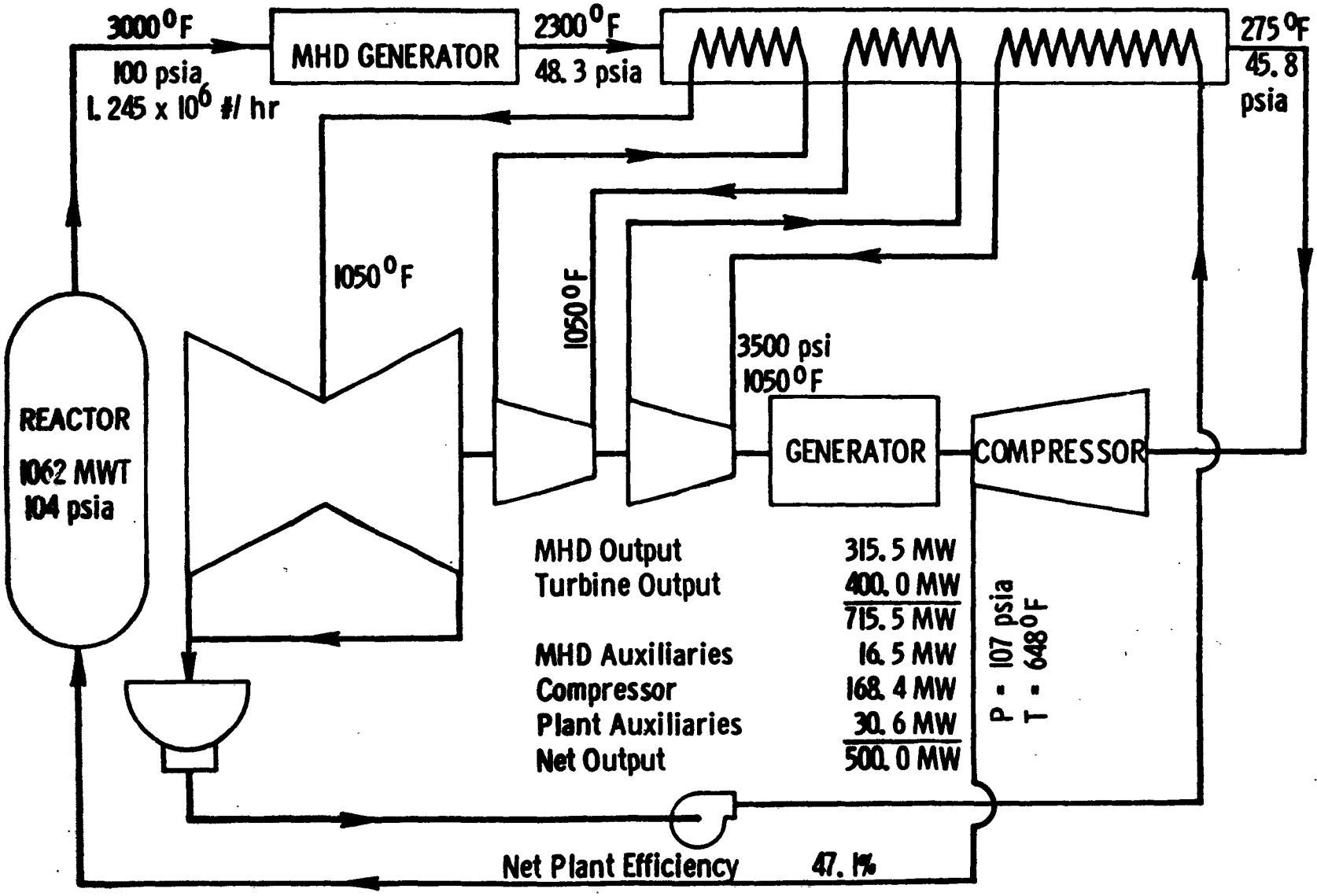

Fig. 4

500 MWe GCR - MHD POWER PLANT

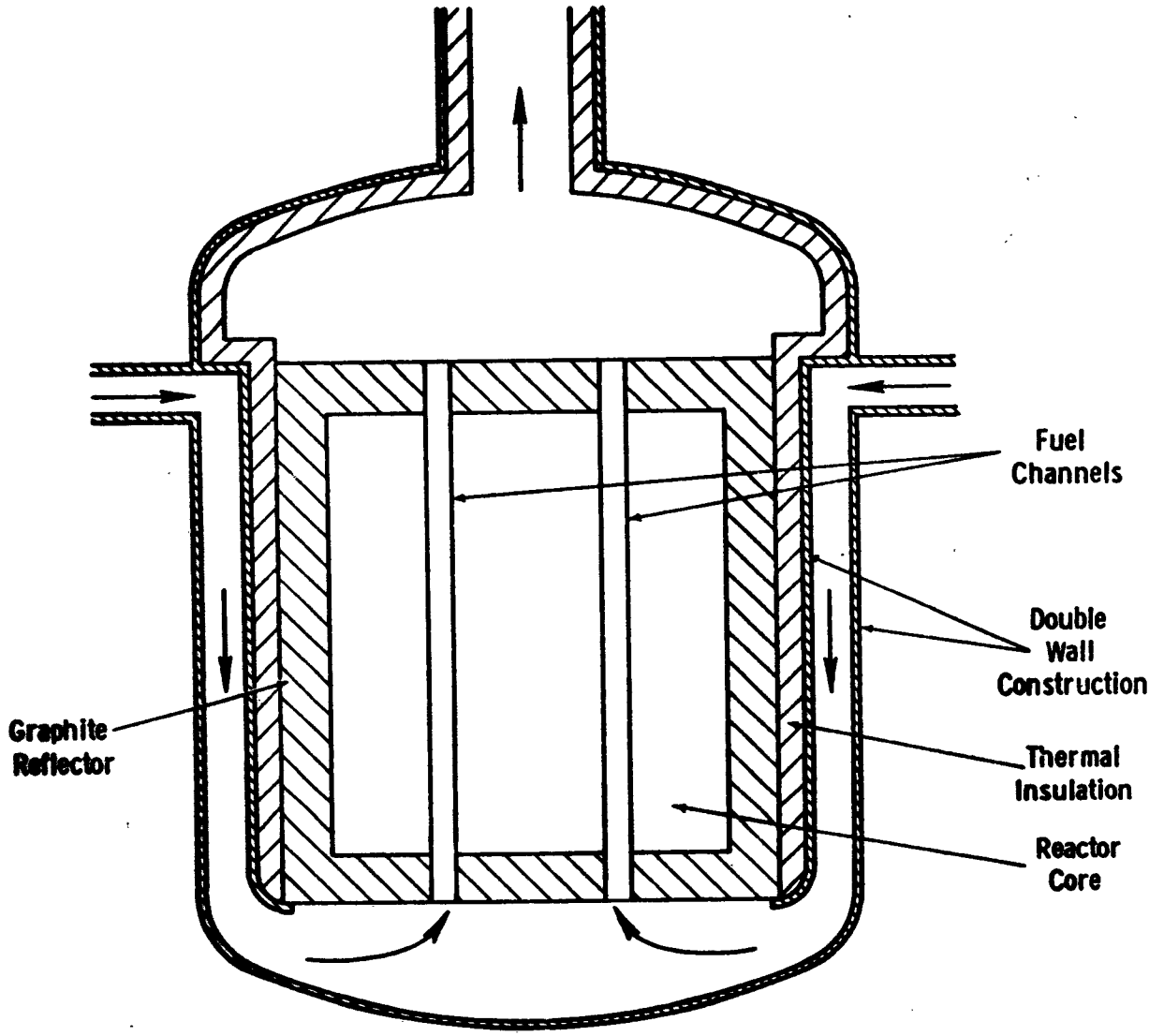

GCR - MHD REACTOR SECTION

E. D. SK 297628 B

Fig. 5

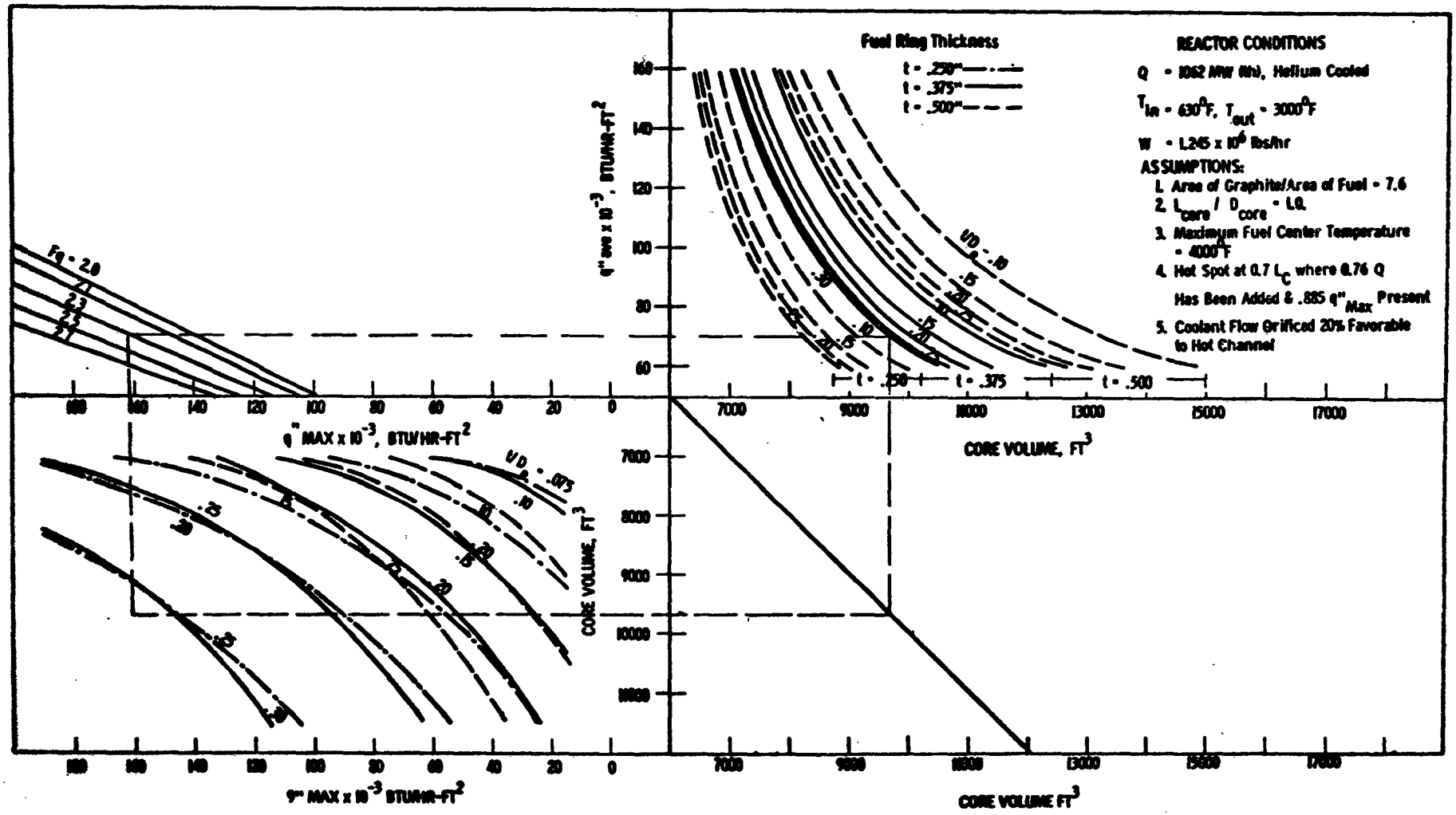

GAS COOLED REACTOR DESIGN PARAMETERS
Fig. 6

E.B. SK. 28998 - C

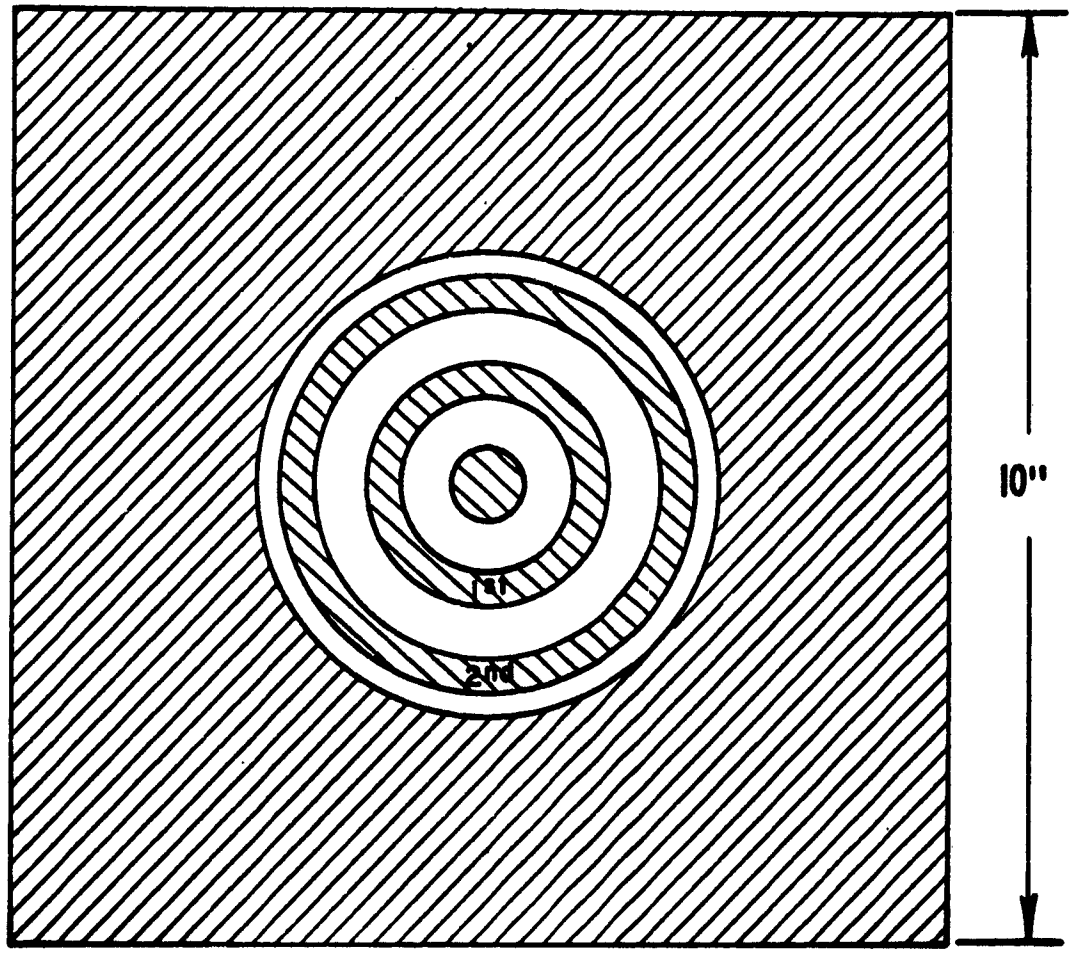

Rod dia	0.750"
Ist ring	I.875 I. D. - 2.625 O. D.
2nd ring	3.750 I. D. - 4.50 O. D.
Hole in block	5.06"

GAS COOLED REACTOR FUEL ELEMENT DESIGN

Fig. 7 E. D. SK. 297635 B

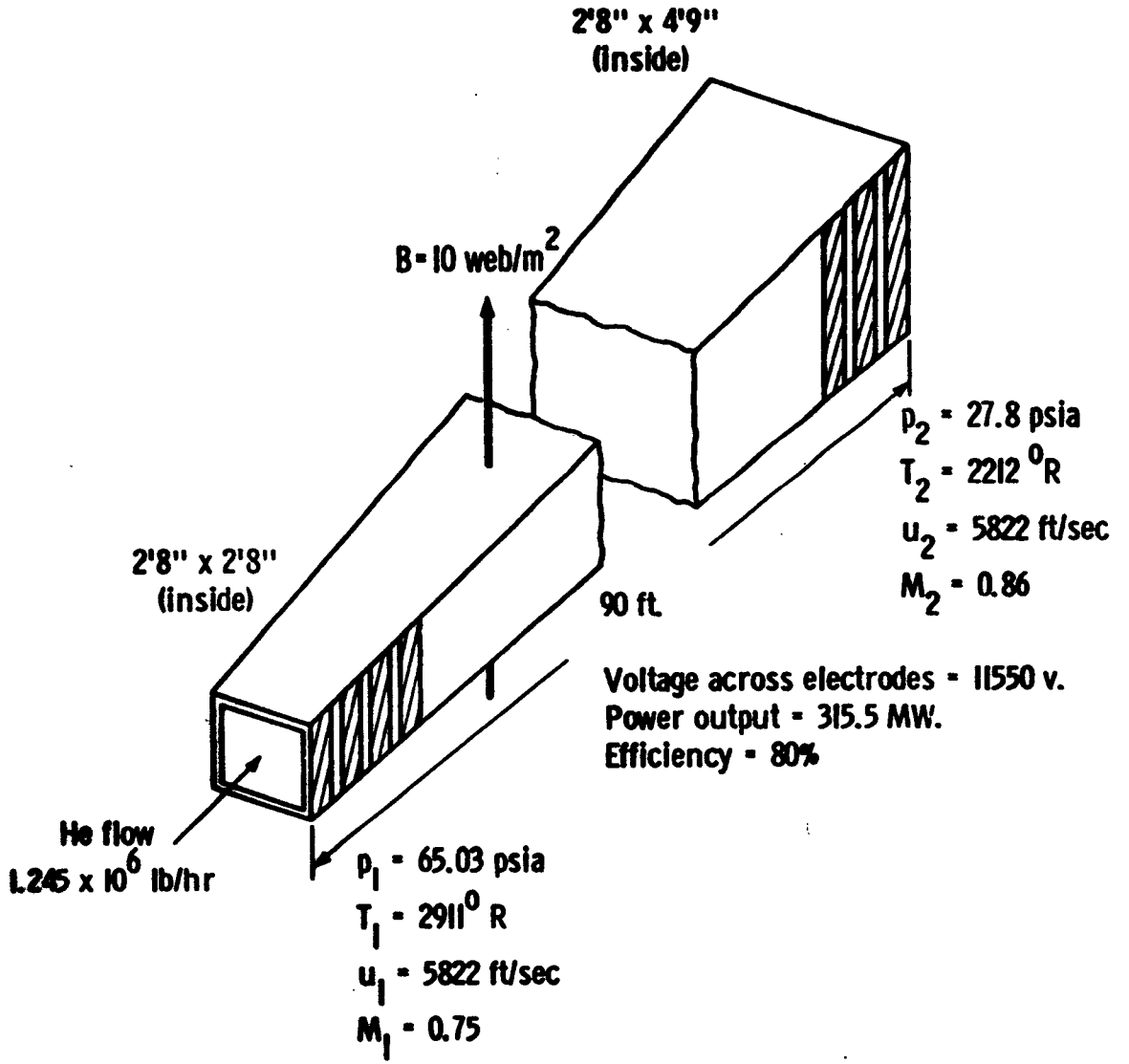

PRINCIPAL CHARACTERISTICS OF MHD GENERATOR

E. D. SK 297629 B

Fig. 8

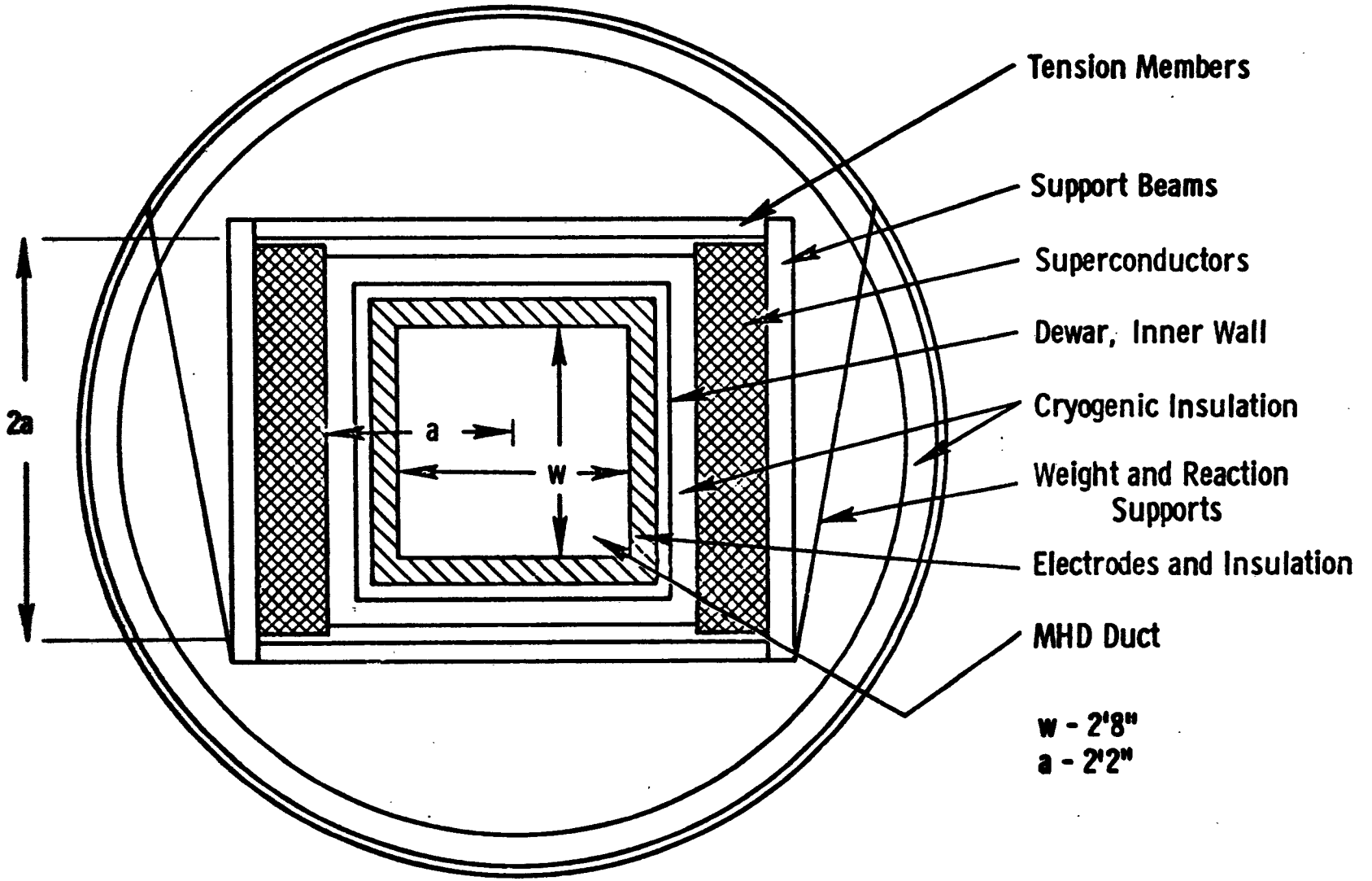

CROSS-SECTION OF MHD DUCT AND MAGNET
Figure 9

E. D. SK. 297637-B

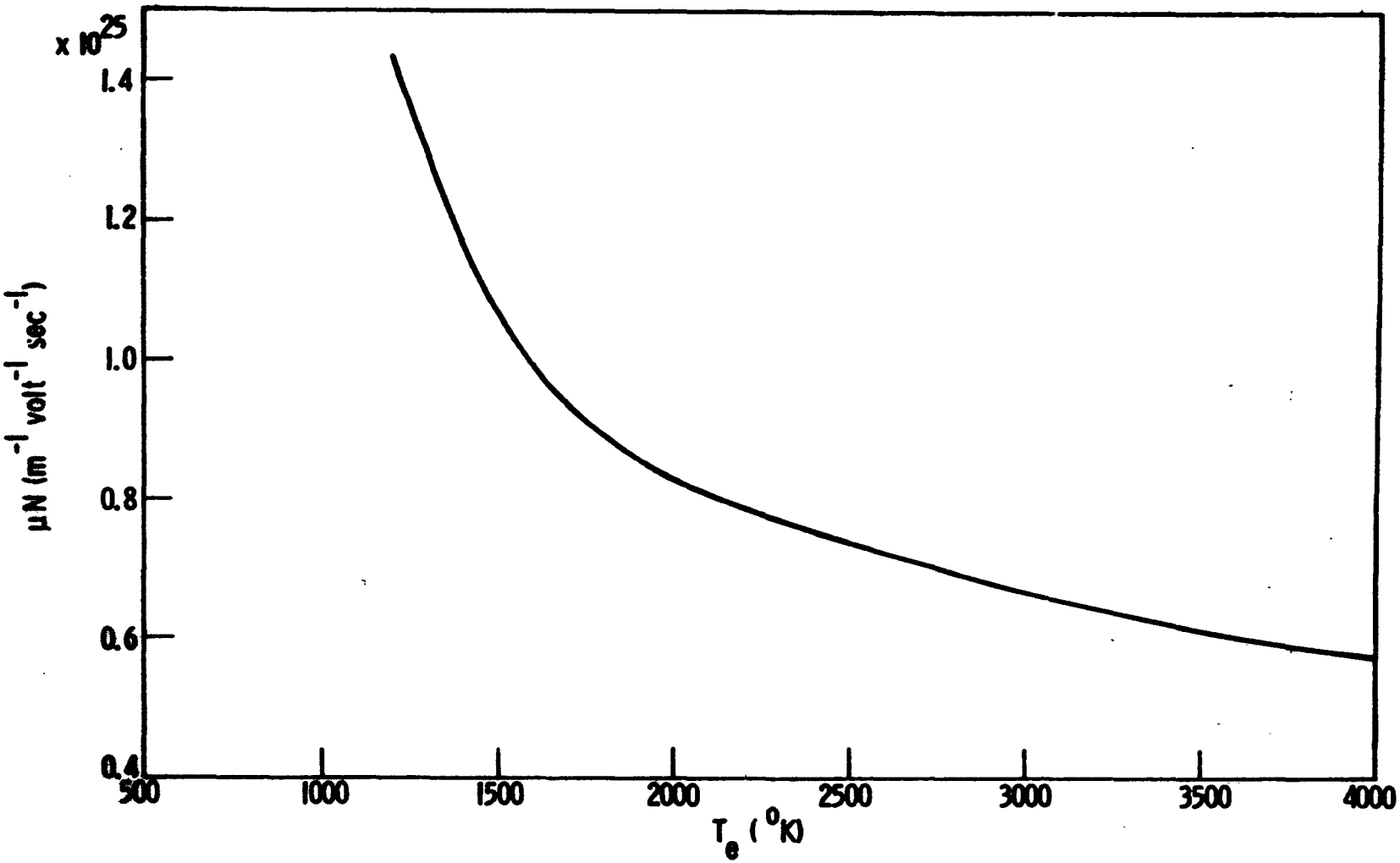

THE PRODUCT OF ELECTRON MOBILITY AND PARTICLE DENSITY AS A FUNCTION OF ELECTRON TEMPERATURE IN PURE HELIUM GAS

Fig. 10

E. D. SK 297632 B

Distribution List

Cys	Activities at WPAFB
1	ASAPT
1	ASAPR
5	ASRMFP-2 (P. J. Hutchison)

Other Dept. of Defense Activities

Navy

Cys	
1	Mr. John A. Satkowski Office of Naval Research Room 2509 Tempo 3 16th and Connecticut Ave. Washington 25, D. C.
1	Dr. H. Powell Jenkins, Jr. Head, Propulsion Applied Research Group (4506) U.S. Naval Ordnance Test Station China Lake, California
1	Mr. B. J. Wilson Naval Research Laboratory Room 322 4th & Chesapeake St., S.W. Washington 25, D. C.

Air Force

Cys	
10	ASTIA (TIPDR) Arlington Hall Arlington 12, Virginia
1	SSD (SSTRE, Captain Hoover) AF Unit Post Office Los Angeles 45, California
1	AFCRL (CRZAP, Dr. N. Rosenberg) L. G. Hanscom Field Bedford, Massachusetts
1	AFOSR (SRHPM, Dr. M. Slawsky) Building T-D Washington 25, D. C.

Cys	Air Force (Cont'd)
1	RADC (RASGP, Mr. Frank J. Mollura) Griffiss Air Force Base, New York

Other U. S. Government Agencies

Cys	
1	Dr. John H. Huth Materials Sciences Office Advanced Research Projects Agency Washington 25, D. C.
1	U. S. Atomic Energy Commission Division of Reactor Development Attn: Cmdr. W. A. Schoenfeld Washington 25, D. C.
1	NASA Lewis Research Center Library 21000 Brookpark Road Cleveland 35, Ohio
1	Mr. Walter Scott Chief, Space Power Tech Program National Aeronautics & Space Administration Washington 25, D. C.
1	U. S. Atomic Energy Commission Office of Technical Information Extension P. O. Box 62 Oak Ridge, Tennessee
1	NASA-Lewis Research Center Electrical Propulsion Office Attn: John Stevens/STEDEMF Cleveland 35, Ohio
1	NASA-Lewis Research Center Plasma Power Generation Section Attn: Lester Nichols Cleveland 35, Ohio

Distribution List (Cont'd)

Non Government Individuals and Organizations

1 Dr. J. E. McCune
Aeronautical Research Associates of Princeton
Princeton, New Jersey

1 Dr. T. Brogan
AVCO-Everett Research Laboratory
2385 Revere Beach
Everett, Massachusetts

1 Dr. J. Cole
Department of Aeronautics
California Institute of Technology
Pasadena, California

1 Mr. Arthur Sherman, Acting Manager
MHD Power Generation
General Electric - Valley Forge
Valley Forge Space Tech Center
Philadelphia 1, Pennsylvania

1 Dr. M. Talaat
Martin Marietta Corporation
Nuclear Division
Baltimore 3, Maryland

1 Professor H. H. Woodson
Electrical Engineering Department
Massachusetts Institute of Tech.
Cambridge 39, Massachusetts

1 Dr. Vernon H. Blackman
MHD Research Incorporated
1535 Monrovia Street
Newport Beach, California

1 Dr. M. C. Gourdine, Chief Scientist
Curtiss-Wright Corporation
Wright-Aeronautical Division
Wood-Ridge, New Jersey

1 Dr. W. O. Carlson
Radio Corporation of America
Defense Electronic Products
Moorestown, New Jersey

1 Dr. Robert Eustis
Thermosciences Division
Stanford University
Stanford, California

1 Mr. Stan Markowski
Pratt and Whitney Aircraft
400 Main Street
East Hartford 8, Connecticut

1 Dr. Richard Schamberg
Rand Corporation
1700 S. Main Street
Santa Monica, California

1 Dr. Sam Naiditch
President
Unified Science Associates
826 Arroyo Parkway
Pasadena, California